Robotica (2022), **40**, pp. 1979–2009
doi:10.1017/S026357472100148X

CAMBRIDGE
UNIVERSITY PRESS

RESEARCH ARTICLE

A nonlinear optimal control approach for underactuated power-line inspection robots

Gerasimos Rigatos[1,*], Nikolaos Zervos[1], Pierluigi Siano[2], Masoud Abbaszadeh[3], Jorge Pomares[4] and Patrice Wira[5]

[1]Unit of Industrial Autom., Industrial Systems Inst., 26504, Rion Patras Greece, [2]Department of Innovation Syst., University of Salerno, Fisciano, 84084, Italy, [3]GE Global Research, General Electric, Niskayuna 12309 NY USA, [4]Dept. of Systems Eng., University of Alicante, 03690 Alicante, Spain and [5]IRIMAS, Université d' Haute Alsace, 68093 Mulhouse, France
*Corresponding author. E-mail: grigat@ieee.org

Received: 12 November 2019; **Revised:** 21 July 2021; **Accepted:** 10 September 2021; **First published online:** 18 October 2021

Keywords: power-line inspection robots, electric grid security, underactuated robots, nonlinear optimal control, H-infinity control, algebraic Riccati equation, Lyapunov stability analysis, global asymptotic stability

Abstract

The article proposes a nonlinear optimal (H-infinity) control approach for a type of underactuated power-line inspection robots. To implement this control scheme, the state-space model of the power-line inspection robots undergoes first approximate linearization around a temporary operating point, through first-order Taylor series expansion and through the computation of the associated Jacobian matrices. To select the feedback gains of the controller an algebraic Riccati equation is solved at each time step of the control method. The global stability properties of the control loop are proven through Lyapunov analysis. The significance of the article's results is outlined in the following: (i) the proposed control method is suitable for treating underactuated robotic systems and in general nonlinear dynamical systems with control inputs gain matrices which are in a nonquadratic form, (ii) by achieving stabilization of the power-line inspection robots in underactuation conditions the proposed control method ensures the reliable functioning of these robotic systems in the case of actuators' failures or enables the complete removal of certain actuators and the reduction of the weight of these robotic systems, (iii) the proposed control method offers a solution to the nonlinear optimal control problem which is of proven global stability while also remaining computationally tractable, (iv) the proposed nonlinear optimal control method retains the advantages of linear optimal control that is fast and accurate tracking of reference setpoints under moderate variations of the control inputs, and (v) by minimizing the amount of energy that is dispersed by the actuators of the power-line inspection robots the proposed control method improves the autonomy and operational capacity of such robotic systems.

1. Introduction

Inspection for faults of power grid components such as cables of the transmission and distribution system and insulators, as well as cleaning and de-icing of these components, is often carried out by humans [1–7]. These are dangerous tasks, taking place in harsh conditions and exposing the life of the maintenance personnel to the risk of fatal accidents. To mitigate such risks and to perform faster and more efficient faults finding and repair in the power grid infrastructure, power-line inspection (PLI) robots can be used [8–14]. The control problem of these robots remains a challenge because of the nonlinearities that characterize the related dynamic model and because of underactuation [15–18]. So far, several approaches have been proposed for solving the nonlinear control problem of PLI robots [19–24]. Stability proof has become a prerequisite in the development of controllers for such robotic mechanisms [25–28]. Backstepping control and sliding mode control are among the nonlinear control methods one can consider for the PLI robots. However, such methods require the state-space model of the robots to be found in a specific form [25]. Furthermore, there exist few results on the nonlinear optimal control of PLI robots and on how energy dissipation by their actuators can be reduced [29, 30].

© The Author(s), 2021. Published by Cambridge University Press.

https://doi.org/10.1017/S026357472100148X Published online by Cambridge University Press

In this article, a novel nonlinear optimal (H-infinity) control method is developed for the dynamic model of an underactuated PLI robot [25]. To this end, the robot's dynamic model undergoes first approximate linearization around a time-varying operating point which is updated at each time step of the control method. Actually, at each sampling period, this operating point is defined by the present value of the robot's state vector and by the last sampled value of the control inputs vector. The linearization relies on first-order Taylor series expansion and on the computation of the related Jacobian matrices [31–33]. The truncation of higher order terms from the Taylor series expansion is considered to be a perturbation that is asymptotically compensated by the robustness of the control method. For the approximately linearized model of the PLI robot, an optimal (H-infinity) feedback controller is designed.

The H-infinity controller provides the solution to the optimal control problem for the PLI robots under model uncertainty and external disturbances [34–36]. It represents a min-max differential game taking place between (i) the control inputs which try to minimize a cost function that comprises a quadratic term of the state vector's tracking error and (ii) the model uncertainty and external perturbations which try to maximize this cost function. To compute the stabilizing feedback gains of the H-infinity controller an algebraic Riccati equation is also solved at each sampling period of the control method [25]. The stability properties of the control loop are proven through Lyapunov analysis. First, it is demonstrated that the control scheme satisfies the H-infinity tracking performance criterion [37, 38]. This signifies elevated robustness against model imprecision and exogenous perturbations. Moreover, under moderate conditions, it is proven that the control loop is globally asymptotically stable. Finally, to implement state estimation-based feedback control of the robot, without the need to measure its entire state vector, the H-infinity Kalman filter is used as a robust state estimator.

The necessity for using robotic systems for inspection and maintenance of the electricity grid is easy to understand since the related tasks expose the repair teams of power corporations to harsh and dangerous conditions with a high risk for fatal accidents [5, 25]. Mainly, the following robotic systems are used for surveillance and repair of the electricity grid: (1) PLI robots suspended from cables, (2) unmanned micro-aerial vehicles, and (3) robotic manipulators and mobile manipulators with hydraulic or electric actuation. Robotic systems carrying out the inspection and maintenance of power lines are amenable to improvement and optimization of their function with respect to the following indicators: (i) precise positioning in the case of model uncertainty, accuracy in tasks execution, dexterity, and maneuverability, (ii) lower power consumption and higher autonomy and operational capacity, and (iii) reliability in underactuation conditions aiming at reduction of the robots' weight and of their design's complexity. With reference to (i) the article develops robust and fault-tolerant control and estimation methods that will preserve the reliable functioning of PLI robots. With reference to (ii) the article's methods reduce energy consumption by PLI robots, thus improving their autonomy and operational capacity and reducing their functioning cost. With reference to (iii), the article's findings allow to simplify the design of the robots used in power-lines inspection and maintenance and to reduce their weight and energy consumption, while also assuring that their accuracy in tasks execution, their maneuverability and their dexterity will remain unaffected.

A distinctive difference to previous results in this area is that the present article achieves a solution of the robot optimal control problem with global stability credentials and without model constraining assumptions. About [39] it can be noted that the considered dynamic model of the 3-DOF wheel inverted pendulum robot is substantially different from the model of the power-lines inspection robot. Actually, the first robotic system exhibits three degrees of freedom and has two control inputs, while the model of the power-lines inspection robot has two degrees of freedom and receives only one control input. In ref. [40], it is attempted to approximate the Hamilton–Jacobi–Bellman equation for the nonlinear optimal control problem with an expansion into Galerkin series. It remains to confirm the global stability properties of this control method and to verify its convergence to the solution of the nonlinear optimal control problem. In ref. [41], a treatment of the nonlinear optimal control problem is attempted for nonlinear affine-in-the-input dynamical systems by assuming once again the decomposition of the solution of the Hamilton–Jacobi–Bellman equation into Galerkin series. It remains to prove global stability and

https://doi.org/10.1017/S026357472100148X Published online by Cambridge University Press

to ensure convergence to the solution of the nonlinear optimal control problem. In ref. [42], a solution of the noninear optimal (H-infinity) control problem for cooperative robotic manipulators is attempted by assuming that the associated state-space model can be written in the linear parameter varying (LPV) form. The LPV assumption does not allow the application of the control method to systems which cannot be brought to the LPV form. In ref. [43] a state-dependent Riccati equation approach (SDRE) is proposed for the solution of the nonlinear optimal control problem in robotic systems. However, the application of the SDRE method is limited to systems which are found into the LPV form. In ref. [43], the use of robots for inspection of critical industrial installations, such as nuclear power plants, is considered. The proposed control scheme that is based on PID controllers may not assure global stability and reliable functioning under non-trivial operating conditions. In ref. [45], an overview is provided about the use of mobile robots in inspection tasks for the electric power transmission and distribution grid. It remains to demonstrate optimal control schemes that reduce energy consumption by such robots. Finally, in ref. [46], mobile robots are proposed for the inspection of power lines in the MV-LV power distribution grid. It can be concluded that the nonlinear control problem of these robots and the associated solutions can be further developed.

The structure of the article is as follows: in Section 2, Euler-Lagrange analysis is applied, and the equations of motion of the PLI robot are obtained. The related state-space model is formulated. In Section 3, the state-space model of the robot undergoes approximate linearization with the use of Tayior series expansion and through the computation of the related Jacobian matrices. In Section 4, the global stability properties of the control scheme are proven through Lyapunov analysis. Furthermore, the H-infinity Kalman filter is presented as a robust state estimator for the PLI robot, which allows for implementing state estimation-based feedback control. Besides an H-infinity feedback controller is developed for the approximately linearized model of the robotic system. In Section 5, the differential flatness properties of the dynamic model of the PLI robot are analyzed and a flatness-based controller is developed for this robotic system. In Section 6, a sliding-mode controller is designed for the model of the power-lines inspection robot and the global stability properties of this control method are proven. In Section 7, the performance of the nonlinear optimal control method is further confirmed and evaluated through simulation experiments. Finally, in Section 8, concluding remarks are stated.

2. Dynamic Model of the PLI Robot

2.1. Computation of the robotic system's Lagrangian

As noted above, one can distinguish three main classes of robotic systems used in the inspection and maintenance of the electricity grid: (1) autonomous robots that are suspended from cable lines, (2) unmanned aerial vehicles and aerial manipulators carrying out inspection tasks, and (3) mobile manipulators and robotic cranes involved also in faults finding and repair in the power grid infrastructure. As far as the first class of robotic systems is concerned, that is robots suspended from cable lines, one can distinguish mainly two-arm and multiarm robots [47–49]. As far as the second class of robotic systems is concerned that is unmanned aerial vehicles and aerial manipulators one can distinguish mainly autonomous helicopters, tricopters, quadropters, hexacopters, and octocopters [50–52]. These types of drones are often turned into aerial manipulators after attaching robotic arms on the aerial platforms. By incorporating robotic manipulators in these aerial platforms several types of unmanned aerial manipulators are obtained. As far as the third class of robotic systems is concerned that is mobile manipulators and robotic cranes once again one comes against several types of such types of robots (comprising different types of mobile platforms and multi-DOF robotic arms) [53, 54].

The specific type of the PLI robot to be analyzed next comes from [1]. The diagram of the underactuated PLI robot is depicted in Figs. 1 and 2. Actually, in Fig. 2, it is considered that the PLI robot has been rotated about its vertical position by an angle θ_1. Then, in the *OXYZ* inertial reference frame, the coordinates of mass m_1 are $x_{m_1} = 0$, $y_{m_1} = -h_1 cos(\theta_1)$ and $z_{m_1} = -h_1 sin(\theta_1)$. In the

https://doi.org/10.1017/S026357472100148X Published online by Cambridge University Press

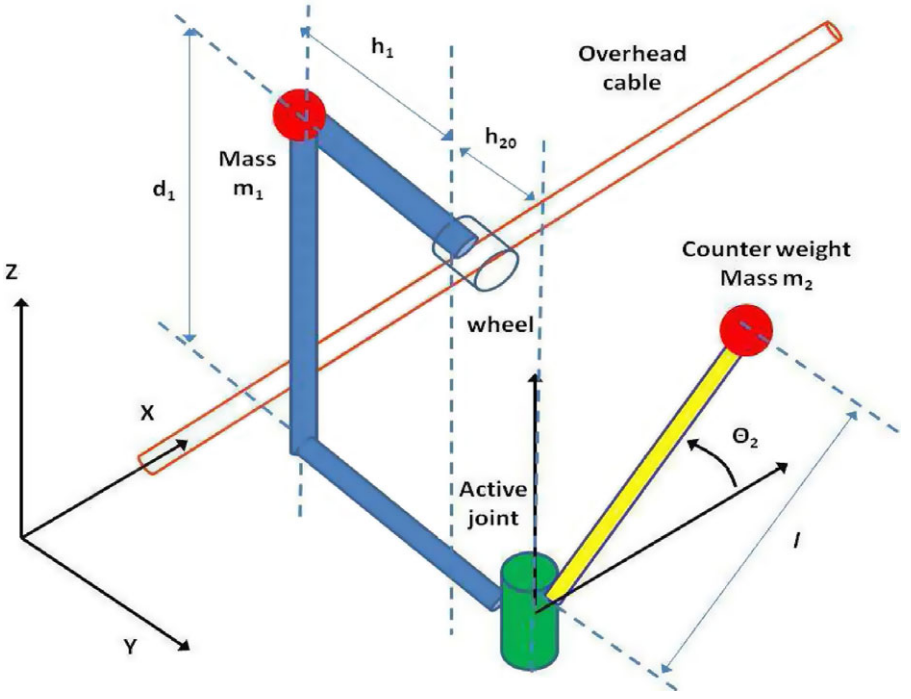


Figure 1. *Diagram of the PLI robot.*

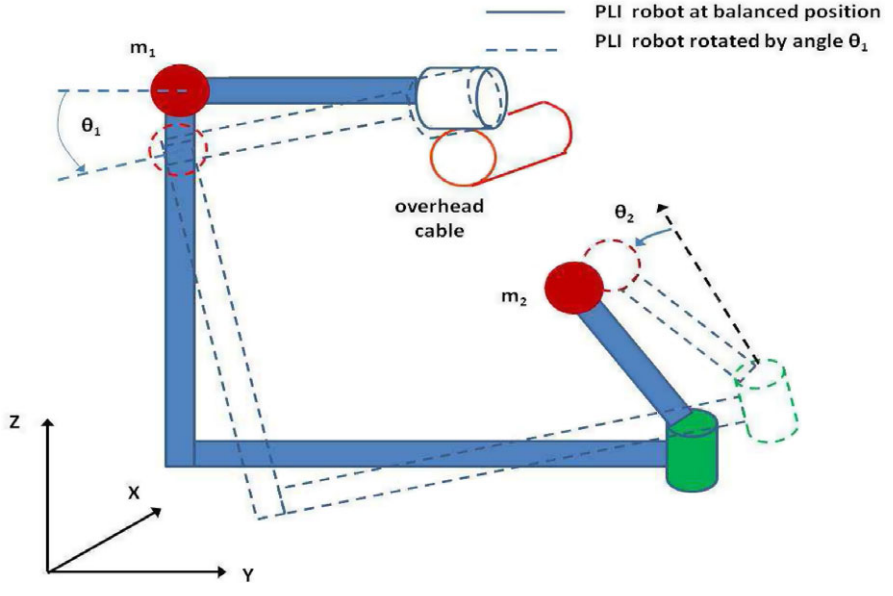


Figure 2. *Rotation of the of the PLI robot by an angle θ_1 from its balanced position and rotation of its counterweight mass m_2 by an angle θ_2.*

same reference frame, the coordinates of the counterweight mass m_2 are given by $x_{m_2} = lcos(\theta_2)$, $y_{m_2} = (h_{20} - lsin(\theta_2))cos(\theta_1) + d_1 sin(\theta_1)$ and $z_{m_2} = (h_{20} - lsin(\theta_2))sin(\theta_1) - d_1 cos(\theta_1)$.

The velocity of mass m_1 is given by

$$\dot{x}_{m_1} = 0 \quad \dot{y}_{m_1} = h_1 sin(\theta_1))\dot{\theta}_1 \quad z_{m_1} = -h_1 cos(\theta_1))\dot{\theta}_1 \tag{1}$$

https://doi.org/10.1017/S026357472100148X Published online by Cambridge University Press

The velocity of mass m_2 is given by

$$\begin{gathered}\dot{x}_{m_2} = -lsin(\theta_2)\dot{\theta}_2 \\ \dot{y}_{m_2} = (-lcos(\theta_2)\dot{\theta}_2)cos(\theta_1) - (h_{20} - lsin(\theta_2))sin(\theta_1)\dot{\theta}_1 + d_1cos(\theta_1)\dot{\theta}_1 \\ \dot{z}_{m_2} = (-lcos(\theta_2)\dot{\theta}_2)sin(\theta_1) + (h_{20} - lsin(\theta_2))cos(\theta_1)\dot{\theta}_1 + d_1sin(\theta_1)\dot{\theta}_1\end{gathered} \tag{2}$$

The kinetic energy due to translation of mass m_1 is

$$\begin{gathered}K_1 = \frac{1}{2}m_1\left(\dot{x}_{m_1}^2 + \dot{y}_{m_1}^2 + \dot{z}_{m_1}^2\right) \Rightarrow \\ K_1 = \frac{1}{2}m_1\left(h_1^2 sin^2(\theta_1)\,\dot{\theta}_1^2 + h_1^2 cos^2(\theta_1)\,\dot{\theta}_1^2\right) \Rightarrow \\ K_1 = \frac{1}{2}m_1 h_1^2 \dot{\theta}_1^2\end{gathered} \tag{3}$$

The kinetic energy due to translation of mass m_2 is

$$\begin{gathered}K_2 = \frac{1}{2}m_2\left(\dot{x}_{m_2}^2 + \dot{y}_{m_2}^2\right) + \dot{z}_{m_2}^2 \Rightarrow \\ K_2 = \frac{1}{2}m_2\{l^2 sin^2(\theta_2)\dot{\theta}_2^2 + l^2 cos^2(\theta_1)cos^2(\theta_2)\dot{\theta}_2^2\} + \\ +[(h_{20} - lsin(\theta_1)sin(\theta_1)) - d_1cos(\theta_1)]^2\dot{\theta}_1^2 - \\ -2[(-lcos(\theta_2))cos(\theta_1)][(h_{20} - lsin(\theta_2))sin(\theta_1) + d_1cos(\theta_1)]\dot{\theta}_1\dot{\theta}_2 \\ +l^2 cos^2(\theta_2)sin^2(\theta_1)\dot{\theta}_2^2 + [(h_{20} - lsin(\theta_2))cos(\theta_1) + d_1sin(\theta)_1]^2\dot{\theta}_1^2 + \\ +2[(-lcos(\theta_2))sin(\theta_1)][(h_{20} - lsin(\theta_2))cos(\theta_1) + d_1sin(\theta_1)]\dot{\theta}_1\dot{\theta}_2\end{gathered} \tag{4}$$

After regrouping terms, one obtains

$$\begin{gathered}K_2 = \frac{1}{2}m_2\{l^2 sin^2(\theta_2)\dot{\theta}_2^2 + l^2 cos^2(\theta_2)\dot{\theta}_2^2 + \\ (h_{20} - lsin(\theta_2))^2\dot{\theta}_1^2 + d_1^2\dot{\theta}_1^2 - \\ -2(-lcos(\theta_2))cos(\theta_1)(h_{20} - lsin(\theta_2))sin(\theta_1)\dot{\theta}_1\dot{\theta}_2 - \\ -2(lcos(\theta_2))cos(\theta_1)d_1cos(\theta_1)\dot{\theta}_1\dot{\theta}_2 + \\ +2(lcos(\theta_2))sin(\theta_1)(h_{20} - lsin(\theta_2))cos(\theta_1)\dot{\theta}_1\dot{\theta}_2 + \\ +2(lcos(\theta_2))sin(\theta_1)d_1cos(\theta_1)\dot{\theta}_1\dot{\theta}_2\}\end{gathered} \tag{5}$$

Through additional operations, one obtains

$$K_2 = \frac{1}{2}m_2\left\{l^2\dot{\theta}_2^2 + (h_{20} - lsin(\theta_1))^2\dot{\theta}_1^2 + d_1^2\dot{\theta}_1^2\right\} \tag{6}$$

Therefore, the total kinetic energy of the robotic mechanism is

$$\begin{gathered}K = K_1 + K_2 \Rightarrow \\ K = \frac{1}{2}m_1 h_1^2\dot{\theta}_1^2 + \frac{1}{2}m_2 l^2\dot{\theta}_2^2 + \frac{1}{2}m_2\left[(h_{20} - lsin(\theta_1))^2 + d_1^2\right]\dot{\theta}_1^2\end{gathered} \tag{7}$$

Next, the potential energy of the robotic mechanism is computed. The potential energy of mass m_1 is

$$\begin{gathered}P_1 = m_1 g z_1 \Rightarrow P_1 = m_1 g(-h_1 sin(\theta_1)) \\ \Rightarrow P_1 = -m_1 g h_1 sin(\theta_1)\end{gathered} \tag{8}$$

https://doi.org/10.1017/S026357472100148X Published online by Cambridge University Press

The potential energy of mass m_2 is

$$\begin{gathered} P_2 = m_2 g z_2 \Rightarrow P_2 = m_2 g[(h_{20} - lsin(\theta_2))sin(\theta_1) - d_1 cos(\theta_1)] \\ \Rightarrow P_1 = -m_1 g h_1 sin(\theta_1) \end{gathered} \tag{9}$$

The aggregate potential energy of the robotic system is given by

$$\begin{gathered} P = P_1 + P_2 \Rightarrow \\ P = -m_1 g h_1 sin(\theta_1) - m_2 g[(h_{20} - lsin(\theta_2))sin(\theta_1) - d_1 cos(\theta_1)] \end{gathered} \tag{10}$$

the Lagrangian of the robotic system is [1, 25]

$$\begin{gathered} L = K - P \Rightarrow \\ L = \frac{1}{2} m_1 h_1^2 \dot{\theta}_1^2 + \frac{1}{2} m_2 l^2 \dot{\theta}_2^2 + \frac{1}{2} m_2 \left[(h_{20} - lsin(\theta_1))^2 + d_1^2\right] \dot{\theta}_1^2 + \\ + m_1 g h_1 sin(\theta_1) + m_2 g \left[(h_{20} - lsin(\theta_2))sin(\theta_1) - d_1 cos(\theta_1)\right] \end{gathered} \tag{11}$$

2.2. State-space model of the PLI robot

The equations that constitute the dynamic model of the power-line inspection robot are obtained from the related Euler–Lagrange equations:

$$\begin{gathered} \frac{\partial}{\partial t} \frac{\partial L}{\partial \dot{\theta}_1} - \frac{\partial L}{\partial \theta_1} = 0 \\ \frac{\partial}{\partial t} \frac{\partial L}{\partial \dot{\theta}_2} - \frac{\partial L}{\partial \theta_2} = u \end{gathered} \tag{12}$$

where u is the torque applied to the actuator of the joint that rotates the counterweight of mass m_2. It holds that

$$\frac{\partial L}{\partial \dot{\theta}_1} = m_1 h_1^2 \dot{\theta}_1 + m_2 [(h_{20} - lsin(\theta_2))^2 + d_1^2] \dot{\theta}_1 \tag{13}$$

Moreover, it holds that

$$\begin{gathered} \frac{d}{dt} \frac{\partial L}{\partial \dot{\theta}_1} = m_1 h_1^2 \ddot{\theta}_1 + m_2 \left[2(h_{20} - lsin(\theta_2))(-lcos(\theta_2))\dot{\theta}_2\right] \dot{\theta}_1 + \\ + m_2 \left[(h_{20} - lsin(\theta_2))^2 + d_1^2\right] \ddot{\theta}_1 \Rightarrow \\ \frac{d}{dt} \frac{\partial L}{\partial \dot{\theta}_1} = \left\{m_1 h_1^2 + m_2 \left[(h_{20} - lsin(\theta_2))^2 + d_1^2\right]\right\} \ddot{\theta}_1 + \\ + m_2 \left[2(h_{20} - lsin(\theta_2))(-lcos(\theta_2))\right] \dot{\theta}_1 \dot{\theta}_2 \end{gathered} \tag{14}$$

Additionally, one has that

$$\frac{\partial L}{\partial \theta_1} = m_1 g h_1 cos(\theta_1) - m_2 g[(h_{20} - lsin(\theta_2))cos(\theta_1) + d_1 sin(\theta_1)] \tag{15}$$

Consequently, the first equation of motion becomes

$$\begin{gathered} \frac{\partial}{\partial t} \frac{\partial L}{\partial \dot{\theta}_1} - \frac{\partial L}{\partial \theta_1} = 0 \Rightarrow \\ \left\{m_1 h_1^2 + m_2 \left[(h_{20} - lsin(\theta_2))^2 + d_1^2\right]\right\} \ddot{\theta}_1 + \\ + m_2 \left[2(h_{20} - lsin(\theta_2))(-lcos(\theta_2))\right] \dot{\theta}_1 \dot{\theta}_2 - \\ - m_1 g h_1 cos(\theta_1) + m_2 g \left[(h_{20} - lsin(\theta_2))cos(\theta_1) + d_1 sin(\theta_1)\right] = 0 \end{gathered} \tag{16}$$

https://doi.org/10.1017/S026357472100148X Published online by Cambridge University Press

Furthermore, one has

$$\frac{\partial L}{\partial \dot{\theta}_2} = m_2 l^2 \dot{\theta}_2 \tag{17}$$

and also

$$\frac{d}{dt}\frac{\partial L}{\partial \dot{\theta}_2} = m_2 l^2 \ddot{\theta}_2 \tag{18}$$

Moreover, it holds that

$$\frac{\partial L}{\partial \theta_2} = m_2(h_{20} - lsin(\theta_2))(-lcos(\theta_2))\dot{\theta}_1^2 - m_2 g(-lcos(\theta_2))sin(\theta_1) \tag{19}$$

Thus, the second equation of motion of the robotic system becomes

$$\begin{gathered}\frac{\partial}{\partial t}\frac{\partial L}{\partial \dot{\theta}_2} - \frac{\partial L}{\partial \theta_2} = u \Rightarrow \\ ml^2\ddot{\theta}_2 + m_2(h_{20} - lsin(\theta_2))(lcos(\theta_2))\dot{\theta}_1^2 - m_2 g(lcos(\theta_2))sin(\theta_1) = u\end{gathered} \tag{20}$$

The following state variables are defined: $x_1 = \theta_1$, $x_2 = \dot{\theta}_1$, $x_3 = \theta_2$ and $x_4 = \dot{\theta}_2$. Consequently, one can obtain the following state-space description:

$$\begin{gathered}\left\{m_1 h_1^2 + m_2[(h_{20} - lsin(x_3))^2 + d_1^2]\right\}\ddot{x}_1 + m_2\left[2(h_{20} - lsin(x_3))(-lcos(x_3))\right]x_2 x_4 - \\ -m_1 g h_1 cos(x_1) + m_2 g\left[(h_{20} - lsin(x_3))cos(x_1) + d_1 sin(x_1)\right] = 0\end{gathered} \tag{21}$$

$$m_2 l^2 \ddot{x}_3 + m_2(h_{20} - lsin(x_3))lcos(x_3)x_2^2 - m_1 g(lcos(x_3))sin(x_1) = u \tag{22}$$

The previous state-space model can be also written as

$$\ddot{x}_1 = \frac{m_2[2(h_{20} - lsin(x_3))(lcos(x_3))]x_2 x_4}{\{m_1 h_1^2 + m_2[(h_{20} - lsin(x_3))^2 +]\}} + \frac{m_1 g h_1 cos(x_1) + m_2 g[(h_{20} - lsin(x_3))cos(x_1) + d_1 sin(x_1)]}{\{m_1 h_1^2 + m_2[(h_{20} - lsin(x_3))^2]\}} \tag{23}$$

$$\ddot{x}_3 = \frac{-m_2(h_{20} - lsin(x_3))lcos(x_3)x_2^2 + m_1 g(lcos(x_3))sin(x_1)}{m_2 l^2} + \frac{u}{m_2 l^2} \tag{24}$$

Additionally, the state-space model of the system can be written as

$$\dot{x}_1 = x_2 \tag{25}$$

$$\dot{x}_2 = \frac{m_2[2(h_{20} - lsin(x_3))(lcos(x_3))]x_2 x_4}{\{m_1 h_1^2 + m_2[(h_{20} - lsin(x_3))^2 +]\}} + \frac{m_1 g h_1 cos(x_1) + m_2 g[(h_{20} - lsin(x_3))cos(x_1) + d_1 sin(x_1)]}{\{m_1 h_1^2 + m_2[(h_{20} - lsin(x_3))^2]\}} \tag{26}$$

$$\dot{x}_3 = x_4 \tag{27}$$

$$\dot{x}_4 = \frac{-m_2(h_{20} - lsin(x_3))lcos(x_3)x_2^2 + m_1 g(lcos(x_3))sin(x_1)}{m_2 l^2} + \frac{u}{m_2 l^2} \tag{28}$$

Furthermore, one can consider the following concise description of the system in vector fields form

$$\dot{x} = f(x) + g(x)u \tag{29}$$

where $x \in R^{4\times 1}$, $f(x) \in R^{4\times 1}$ and $g(x) \in R^{4\times 1}$ while $u \in R$, or equivalently

$$\begin{pmatrix}\dot{x}_1 \\ \dot{x}_2 \\ \dot{x}_3 \\ \dot{x}_4\end{pmatrix} = \begin{pmatrix}f_1(x) \\ f_2(x) \\ f_3(x) \\ f_4(x)\end{pmatrix} + \begin{pmatrix}g_1(x) \\ g_2(x) \\ g_3(x) \\ g_4(x)\end{pmatrix} u \tag{30}$$

https://doi.org/10.1017/S026357472100148X Published online by Cambridge University Press

where $f_1(x) = x_2, f_2(x) = \frac{m_2[2(h_{20}-lsin(x_3))(lcos(x_3))]x_2x_4}{\{m_1h_1^2+m_2[(h_{20}-lsin(x_3))^2+]\}} + \frac{m_1gh_1cos(x_1)+m_2g[(h_{20}-lsin(x_3))cos(x_1)+d_1sin(x_1)]}{\{m_1h_1^2+m_2[(h_{20}-lsin(x_3))^2]\}}$
$f_3(x) = x_4, f_4(x) = \frac{f_{4n}(x)}{f_{4d}(x)} = \frac{-m_2(h_{20}-lsin(x_3))lcos(x_3)x_2^2+m_1g(lcos(x_3))sin(x_1)}{m_2l^2}$
and $g_1(x) = 0$, $g_2(x) = 0$, $g_3(x) = 0$ and $g_4(x) = \frac{1}{m_2l^2}$.

3. Approximate Linearization of the Power-line Inspection Robot

3.1. Approximately linearized model

The dynamic model of the PLI robot $\dot{x} = f(x) + g(x)u$ undergoes approximate linearization around the time-varying operating point (x^*, u^*), where x^* is the present value of the system's state vector and u^* is the last sampled value of the control inputs vector. The linearization relies on first-order Taylor series expansion and on the computation of the related Jacobian matrices.

This concept results into the approximately linearized model of the robotic system in the form:

$$\dot{x} = Ax + Bu + \tilde{d} \tag{31}$$

where $\tilde{d}$ is the cumulative perturbations' vector which comprises (i) the modeling error due to truncation of higher-order terms in the Taylor series expansion, (ii) external disturbances, and (iii) measurement noise of any distribution.

The Jacobian matrices of the robotic system are

$$A = \nabla_x[f(x) + g(x)u] \mid_{(x^*,u^*)} \Rightarrow A = \nabla_x[f(x)] \mid_{(x^*,u^*)} + \nabla_x[g(x)]u \mid_{(x^*,u^*)} \Rightarrow$$
$$A = \nabla_x[f(x)] \mid_{(x^*,u^*)} \tag{32}$$

$$B = \nabla_u[f(x) + g(x)u] \mid_{(x^*,u^*)} \Rightarrow B = g(x) \mid_{(x^*,u^*)} \tag{33}$$

Next, the elements of the Jacobian matrix $\nabla_x[f(x)] \mid_{(x^*,u^*)}$ are computed.
First row of the Jacobian matrix $\nabla_x[f(x)] \mid_{(x^*,u^*)}$: $\frac{\partial f_1}{\partial x_1} = 0$, $\frac{\partial f_1}{\partial x_2} = 1$, $\frac{\partial f_1}{\partial x_3} = 0$ and $\frac{\partial f_1}{\partial x_4} = 0$.
Second row of the Jacobian matrix $\nabla_x[f(x)] \mid_{(x^*,u^*)}$: for $i = 1, \cdots, 4$

$$\frac{\partial f_2}{\partial x_i} = \frac{\frac{\partial f_{2n}(x)}{\partial x_i} f_{2d}(x) - f_{2n}(x)\frac{\partial f_{2d}(x)}{\partial x_i}}{f_{2d}(x)^2} \tag{34}$$

where $\frac{\partial f_{2n}}{\partial x_1} = m_1gh_1(-sin(x_1)) + m_2g[-(h_{20} + lsin(x_3))sin(x_1) + d_1cos(x_1)]$, $\frac{\partial f_{2n}}{\partial x_2} = m_2[2(h_{20} - lsin(x_3))(lcos(x_3))]x_4$, $\frac{\partial f_{2n}}{\partial x_3} = 2m_2[(-lcos(x_3))(lcos(x_3))]x_2x_4 - 2m_2(h_{20} - lsin(x_3))(lsin(x_3))x_2x_4 + m_2g[(lcos(x_3))cos(x_1)]$, $\frac{\partial f_{2n}}{\partial x_4} = m_2[2(h_{20} - lsin(x_3))(lcos(x_3))]x_2$.

and also $\frac{\partial f_{2d}}{\partial x_1} = 0$, $\frac{\partial f_{2d}}{\partial x_1 2} = 0$, $\frac{\partial f_{2d}}{\partial x_3} = m_2 2(h_{20} - lsin(x_3))(-lcos(x_3))$, $\frac{\partial f_{2d}}{\partial x_4} = 0$.

Third row of the Jacobian matrix $\nabla_x[f(x)] \mid_{(x^*,u^*)}$: $\frac{\partial f_3}{\partial x_1} = 0$, $\frac{\partial f_3}{\partial x_2} = 0$, $\frac{\partial f_3}{\partial x_3} = 0$ and $\frac{\partial f_3}{\partial x_4} = 1$.

Fourth row of the Jacobian matrix $\nabla_x[f(x)] \mid_{(x^*,u^*)}$: $\frac{\partial f_4(x)}{\partial x_1} = \frac{1}{m_2l^2}(m_2g(lcos(x_3))cos(x_1))$, $\frac{\partial f_4(x)}{\partial x_2} = -\frac{2x_2}{m_2l^2}$, $\frac{\partial f_4(x)}{\partial x_3} = \frac{1}{m_2l^2}[-m_2(-lcos(x_3))(lcos(x_3))x_2^2 - m_2(h_{20} - lsin(x_3))(-lsin(x_3))x_2^2 - m_2g(lsin(x_3))sin(x_1)]$, and $\frac{\partial f_4(x)}{\partial x_3} = 0$

3.2. Stabilizing feedback control

After linearization around its current operating point, the dynamic model of the PLI robot is written as

$$\dot{x} = Ax + Bu + d_1 \tag{35}$$

Parameter d_1 stands for the linearization error in the PLI robot's dynamic model appearing previously in Eq. (31). The reference setpoints for the PLI robot's state vector are denoted by $\mathbf{x_d} = [x_1^d, \cdots, x_4^d]$. Tracking of this trajectory is achieved after applying the control input u_d. At every time instant, the

https://doi.org/10.1017/S026357472100148X Published online by Cambridge University Press

control input u_d is assumed to differ from the control input u appearing in Eq. (35) by an amount equal to Δu, that is $u_d = u + \Delta u$

$$\dot{x}_d = Ax_d + Bu_d + d_2 \tag{36}$$

The dynamics of the controlled system described in Eq. (35) can be also written as

$$\dot{x} = Ax + Bu + Bu_d - Bu_d + d_1 \tag{37}$$

and by denoting $d_3 = -Bu_d + d_1$ as an aggregate disturbance term one obtains

$$\dot{x} = Ax + Bu + Bu_d + d_3 \tag{38}$$

By subtracting Eq. (36) from Eq. (38) one has

$$\dot{x} - \dot{x}_d = A(x - x_d) + Bu + d_3 - d_2 \tag{39}$$

By denoting the tracking error as $e = x - x_d$ and the aggregate disturbance term as $\tilde{d} = d_3 - d_2$, the tracking error dynamics becomes

$$\dot{e} = Ae + Bu + \tilde{d} \tag{40}$$

For the approximately linearized model of the system a stabilizing feedback controller is developed. The controller has the form

$$u(t) = -Ke(t) \tag{41}$$

with $K = \frac{1}{r}B^T P$ where P is a positive definite symmetric matrix which is obtained from the solution of the Riccati equation [25]

$$A^T P + PA + Q - P\left(\frac{2}{r}BB^T - \frac{1}{\rho^2}LL^T\right)P = 0 \tag{42}$$

where Q is a positive semi-definite symmetric matrix. The diagram of the considered control loop is depicted in Fig. 3. Clear metrics can be provided about the robustness properties of the proposed nonlinear optimal (H-infinity) control scheme for PLI robots. The solution of the H-infinity feedback control problem for the underactuated PLI robot and the computation of the worst case disturbance that the related controller can sustain, comes from superposition of Bellman's optimality principle when considering that the robot is affected by two separate inputs (i) the control input u (ii) the cumulative disturbance input $\tilde{d}(t)$. Solving the optimal control problem for u, that is for the minimum variation (optimal) control input that achieves elimination of the state vector's tracking error, gives $u = -\frac{1}{r}B^T Pe$. Equivalently, solving the optimal control problem for $\tilde{d}$, that is for the worst case disturbance that the control loop can sustain gives $\tilde{d} = \frac{1}{\rho^2}L^T Pe$. The attenuation coefficient ρ can be given a small value up to the point that the method's algebraic Riccati equation still returns a valid solution in the form of the positive definite and symmetric matrix P. The smallest value of ρ for which a valid solution of the method's algebraic Riccati equation can be obtained (in the form of a positive definite and symmetric matrix P) is the one that provides maximum robustness to the control loop.

The present article provides one of the few existing solutions to the nonlinear optimal control problem of PLI robots which is of proven global stability while also remaining computationally efficient. Preceding results on the use of H-infinity control to nonlinear dynamical systems were limited to the case of affine-in-the-input systems with drift-only dynamics and considered that the control inputs gain matrix is not dependent on the values of the system's state vector. Moreover, in these approaches, the linearization was performed around points of the desirable trajectory, whereas in the present article's control method the linearization points are related with the value of the state vector at each sampling instance as well as with the last sampled value of the control inputs vector. The Riccati equation which has been proposed for computing the feedback gains of the controller is novel, so is the presented global stability proof through Lyapunov analysis. The article's approach enables a solution of the nonlinear optimal control problem without the need to solve state dependent Riccati equations (SDREs).

https://doi.org/10.1017/S026357472100148X Published online by Cambridge University Press

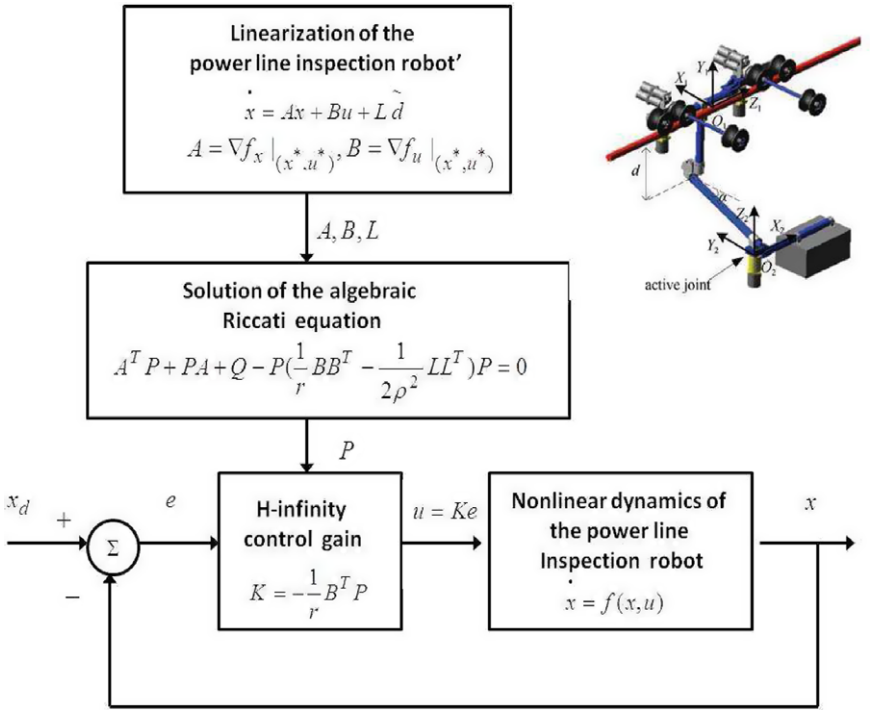


Figure 3. *Diagram of the control scheme for the power-line inspection robot (the figure of the PLI robot comes from [1])*

The article's scientific contribution is outlined as follows: (i) the presented nonlinear optimal control method has improved performance when compared against other nonlinear control schemes that one can consider for the dynamic model of the PLI robots (such as Lie algebra-based control, differential flatness theory-based control, model-based predictive control, nonlinear model-based predictive control, sliding-mode control, backstepping control), etc., (ii) it achieves fast and accurate tracking of all reference setpoints for the PLI robots under moderate variations of the control inputs, and (iii) it minimizes the consumption of energy by the actuators of the PLI robots, thus improving the functioning cost and efficiency in tasks' execution by such robotic systems.

4. Lyapunov Stability Analysis

4.1. Stability proof

Through Lyapunov stability analysis, it will be shown that the proposed nonlinear optimal control scheme, which was formulated in Section 3, assures H_∞ tracking performance for the underactuated PLI robot and that in case of bounded disturbance terms asymptotic convergence to the reference setpoints is achieved. The tracking error dynamics for the PLI robot is written in the form [25]

$$\dot{e} = Ae + Bu + L\tilde{d} \tag{43}$$

where in the PLI robot's case $L \in R^{4\times 4}$ is the disturbance inputs gain matrix. Variable $\tilde{d}$ denotes model uncertainties and external disturbances of the PLI robot's model. The following Lyapunov equation is considered

$$V = \frac{1}{2}e^T Pe \tag{44}$$

https://doi.org/10.1017/S026357472100148X Published online by Cambridge University Press

where $e = x - x_d$ is the tracking error. By differentiating with respect to time one obtains

$$\dot{V} = \frac{1}{2}\dot{e}^T Pe + \frac{1}{2}e^T P\dot{e} \Rightarrow$$
$$\dot{V} = \frac{1}{2}\left[Ae + Bu + L\tilde{d}\right]^T Pe + \frac{1}{2}e^T P\left[Ae + Bu + L\tilde{d}\right] \Rightarrow \tag{45}$$

$$\dot{V} = \frac{1}{2}\left[e^T A^T + u^T B^T + \tilde{d}^T L^T\right]Pe +$$
$$+\frac{1}{2}e^T P\left[Ae + Bu + L\tilde{d}\right] \Rightarrow \tag{46}$$

$$\dot{V} = \frac{1}{2}e^T A^T Pe + \frac{1}{2}u^T B^T Pe + \frac{1}{2}\tilde{d}^T L^T Pe +$$
$$\frac{1}{2}e^T PAe + \frac{1}{2}e^T PBu + \frac{1}{2}e^T PL\tilde{d} \tag{47}$$

The previous equation is rewritten as

$$\dot{V} = \frac{1}{2}e^T\left(A^T P + PA\right)e + \left(\frac{1}{2}u^T B^T Pe + \frac{1}{2}e^T PBu\right) +$$
$$+\left(\frac{1}{2}\tilde{d}^T L^T Pe + \frac{1}{2}e^T PL\tilde{d}\right) \tag{48}$$

Assumption: For given positive definite matrix Q and coefficients r and ρ there exists a positive definite matrix P, which is the solution of the following matrix equation

$$A^T P + PA = -Q + P\left(\frac{2}{r}BB^T - \frac{1}{\rho^2}LL^T\right)P \tag{49}$$

Moreover, the following feedback control law is applied to the system

$$u = -\frac{1}{r}B^T Pe \tag{50}$$

By substituting Eqs. (49) and (50), one obtains

$$\dot{V} = \frac{1}{2}e^T\left[-Q + P\left(\frac{2}{r}BB^T - \frac{1}{\rho^2}LL^T\right)P\right]e +$$
$$+e^T PB\left(-\frac{1}{r}B^T Pe\right) + e^T PL\tilde{d} \Rightarrow \tag{51}$$

$$\dot{V} = -\frac{1}{2}e^T Qe + \frac{1}{r}e^T PBB^T Pe - \frac{1}{2\rho^2}e^T PLL^T Pe$$
$$-\frac{1}{r}e^T PBB^T Pe + e^T PL\tilde{d} \tag{52}$$

which after intermediate operations gives

$$\dot{V} = -\frac{1}{2}e^T Qe - \frac{1}{2\rho^2}e^T PLL^T Pe + e^T PL\tilde{d} \tag{53}$$

or, equivalently

$$\dot{V} = -\frac{1}{2}e^T Qe - \frac{1}{2\rho^2}e^T PLL^T Pe +$$
$$+\frac{1}{2}e^T PL\tilde{d} + \frac{1}{2}\tilde{d}^T L^T Pe \tag{54}$$

https://doi.org/10.1017/S026357472100148X Published online by Cambridge University Press

Lemma: The following inequality holds

$$\frac{1}{2}e^T L\tilde{d} + \frac{1}{2}\tilde{d}L^T Pe - \frac{1}{2\rho^2}e^T PLL^T Pe \leq \frac{1}{2}\rho^2\tilde{d}^T\tilde{d} \tag{55}$$

Proof: The binomial $(\rho\alpha - \frac{1}{\rho}b)^2$ is considered. Expanding the left part of the above inequality one gets

$$\begin{aligned} &\rho^2a^2 + \frac{1}{\rho^2}b^2 - 2ab \geq 0 \Rightarrow \frac{1}{2}\rho^2a^2 + \frac{1}{2\rho^2}b^2 - ab \geq 0 \Rightarrow \\ &ab - \frac{1}{2\rho^2}b^2 \leq \frac{1}{2}\rho^2a^2 \Rightarrow \frac{1}{2}ab + \frac{1}{2}ab - \frac{1}{2\rho^2}b^2 \leq \frac{1}{2}\rho^2a^2 \end{aligned} \tag{56}$$

The following substitutions are carried out: $a = \tilde{d}$ and $b = e^T PL$ and the previous relation becomes

$$\frac{1}{2}\tilde{d}^T L^T Pe + \frac{1}{2}e^T PL\tilde{d} - \frac{1}{2\rho^2}e^T PLL^T Pe \leq \frac{1}{2}\rho^2\tilde{d}^T\tilde{d} \tag{57}$$

Eq. (57) is substituted in Eq. (54) and the inequality is enforced, thus giving

$$\dot{V} \leq -\frac{1}{2}e^T Qe + \frac{1}{2}\rho^2\tilde{d}^T\tilde{d} \tag{58}$$

Eq. (58) shows that the H_∞ tracking performance criterion is satisfied. The integration of $\dot{V}$ from 0 to T gives

$$\begin{aligned} &\int_0^T \dot{V}(t)dt \leq -\frac{1}{2}\int_0^T ||e||_Q^2 dt + \frac{1}{2}\rho^2\int_0^T ||\tilde{d}||^2 dt \Rightarrow \\ &2V(T) + \int_0^T ||e||_Q^2 dt \leq 2V(0) + \rho^2\int_0^T ||\tilde{d}||^2 dt \end{aligned} \tag{59}$$

Moreover, if there exists a positive constant $M_d > 0$ such that

$$\int_0^\infty ||\tilde{d}||^2 dt \leq M_d \tag{60}$$

then one gets

$$\int_0^\infty ||e||_Q^2 dt \leq 2V(0) + \rho^2 M_d \tag{61}$$

Thus, the integral $\int_0^\infty ||e||_Q^2 dt$ is bounded. Moreover, $V(T)$ is bounded and from the definition of the Lyapunov function V in Eq. (44) it becomes clear that $e(t)$ will be also bounded since $e(t) \in \Omega_e = \{e | e^T Pe \leq 2V(0) + \rho^2 M_d\}$. According to the above and with the use of Barbalat's Lemma one obtains $\lim_{t\to\infty} e(t) = 0$.

Elaborating on the stability analysis up to Eq. (61), it can be noted that the proof of global asymptotic stability for the control loop of the power-lines inspection robot is based on Eq. (58) and on the application of Barbalat's Lemma. It uses the condition about the boundedness of the square of the aggregate disturbance and modelling error term $\tilde{d}$ that affects the model. However, as explained in the previous stability analysis, the proof of global asymptotic stability is not restricted by this condition. By selecting the attenuation coefficient ρ to be sufficiently small and in particular to satisfy $\rho^2 < ||e||_Q^2 / ||\tilde{d}||^2$ one has that the first derivative of the Lyapunov function is upper bounded by 0. Therefore, for the ith time interval it is proven that the Lyapunov function defined in Eq (44) is a decreasing one. This also assures that the Lyapunov function of the system defined in Eq. (29) will always have a negative first-order derivative.

4.2. Robust state estimation with the use of the H_∞ Kalman filter

The control loop has to be implemented with the use of information provided by a small number of sensors and by processing only a small number of state variables. To reconstruct the missing information

https://doi.org/10.1017/S026357472100148X Published online by Cambridge University Press

about the state vector of the PLI robot it is proposed to use a filtering scheme and based on it to apply state estimation-based control [37]. The recursion of the H_∞ Kalman filter, for the model of the PLI robot, can be formulated in terms of a *measurement update* and a *time update* part

Measurement update:

$$\begin{aligned} D(k) &= [I - \theta W(k)P^-(k) + C^T(k)R(k)^{-1}C(k)P^-(k)]^{-1} \\ K(k) &= P^-(k)D(k)C^T(k)R(k)^{-1} \\ \hat{x}(k) &= \hat{x}^-(k) + K(k)[y(k) - C\hat{x}^-(k)] \end{aligned} \tag{62}$$

Time update:

$$\begin{aligned} \hat{x}^-(k+1) &= A(k)x(k) + B(k)u(k) \\ P^-(k+1) &= A(k)P^-(k)D(k)A^T(k) + Q(k) \end{aligned} \tag{63}$$

where it is assumed that parameter θ is sufficiently small to assure that the covariance matrix $P^-(k)^{-1} - \theta W(k) + C^T(k)R(k)^{-1}C(k)$ will be positive definite. When $\theta = 0$ the H_∞ Kalman filter becomes equivalent to the standard Kalman filter. One can measure only a part of the state vector of the PLI robot, for instance state variables x_1 (the tilt angle of the robot's body with reference to its vertical position) and x_3 (the angle between the initial and active positions of the actuator's bar), and can estimate through filtering the rest of the state vector elements. Moreover, the proposed Kalman filtering method can be used for sensor fusion purposes.

5. Differential Flatness Properties of the Power-line Inspection (PLI) Robot

5.1. Proof of differential flatness properties for the PLI robot

The dynamic model of the PLI robot was shown to be consisting of the state-space equations given in Eqs. (25)–(28). In its initial nonlinear state-space form this robotic system is not differentially flat [25, 37]. However, for the dynamic model which is obtained after partial linearization around operating point $x^* = [x_1^*, 0, 0, 0]^T$ where x_1^* is piecewise constant, it can be shown that differential flatness properties hold. Following the previously explained procedure about the computation of the robot's Jacobian matrices at the operating point x^*, and the approach presented in [1], one gets:

$$\begin{pmatrix} \dot{x}_1 \\ \dot{x}_2 \\ \dot{x}_3 \\ \dot{x}_4 \end{pmatrix} = \begin{pmatrix} 0 & 1 & 0 & 0 \\ \frac{\partial f_2}{\partial x_1}|_{x^*} & 0 & \frac{\partial f_2}{\partial x_3}|_{x^*} & 0 \\ 0 & 0 & 0 & 1 \\ \frac{\partial f_4}{\partial x_1}|_{x^*} & 0 & 0 & 0 \end{pmatrix} \begin{pmatrix} x_1 \\ x_2 \\ x_3 \\ x_4 \end{pmatrix} + \begin{pmatrix} 0 \\ 0 \\ 0 \\ g_4 \end{pmatrix} u \tag{64}$$

or equivalently, the state-space equations of the power-line inspection robot are written as

$$\begin{aligned} \dot{x}_1 &= x_2 \\ \dot{x}_2 &= \frac{\partial f_2}{\partial x_1}|_{x^*} x_1 + \frac{\partial f_2}{\partial x_3}|_{x^*} x_3 \\ \dot{x}_3 &= x_4 \\ \dot{x}_4 &= \frac{\partial f_4}{\partial x_1}|_{x^*} x_1 + g_4 u \end{aligned} \tag{65}$$

where $\frac{\partial f_2}{\partial x_i}|_{x^*} = \frac{\frac{\partial f_{2n}}{\partial x_1}}{f_{2d}}$ which is a function of x_1, $\frac{\partial f_2}{\partial x_3}|_{x^*} = \frac{\frac{\partial f_{2n}}{\partial x_3} f_{2d} - f_{2n}\frac{\partial f_{2d}}{\partial x_3}}{f_{2d}^2}|_{x^*}$ which is a function of x_1 and $\frac{\partial f_4}{\partial x_1}|_{x^*} = \frac{1}{m_2 l^2}(m_2 g l cos(x_1))$.

with $\frac{\partial f_{2n}}{\partial x_1}|_{x^*} = m_1 g h_1(-sin(x_1)) + m_2 g[-h_{20}sin(x_1) + d_1 cos(x_1)]$, $\frac{\partial f_{2d}}{\partial x_1}|_{x^*} = 0$, $\frac{\partial f_{2n}}{\partial x_3}|_{x^*} = m_2 g cos(x_1)$, $\frac{\partial f_{2d}}{\partial x_3}|_{x^*} = m_2 2 h_{20} l 0$, $f_{2n}|_{x^*} = (m_1 g h_1 + m_2 g h_{20})cos(x_1) + d_1 sin(x_1)$, and $f_{2d}|_{x^*} = m_1 h_1^2 + m_2 h_{20}^2$.

https://doi.org/10.1017/S026357472100148X Published online by Cambridge University Press

It can be proven that the model of Eq. (65) is differentially flat, with flat output $y = x_1$ [25, 37]. From the first row of the state-space model of Eq. (65) one has that

$$x_2 = \dot{x}_1 \Rightarrow x_2 = h_2(y, \dot{y}) \tag{66}$$

which signifies that state variable x_2 is a differential function of the flat output of this robotic system. From the second row of the state-space model of Eq. (65) one has that

$$x_3 = \frac{\dot{x}_2 - \frac{\partial f_2}{\partial x_1} |_{x^*} x_1}{\frac{\partial f_2}{\partial x_3} |_{x^*}} \Rightarrow x_3 = h_3(y, \dot{y}, \ddot{y}) \tag{67}$$

which signifies that state variable x_3 is a differential function of the flat output of this robotic system. From the third row of the state-space model of Eq. (65) one has that

$$x_4 = \dot{x}_3 \Rightarrow x_4 = h_4(y, \dot{y}, \ddot{y}, y^{(3)}) \tag{68}$$

which signifies that state variable x_4 is a differential function of the flat output of this robotic system. Finally, from the fourth row of the state-space model of Eq. (65) one has that

$$u = \frac{1}{g_4}\left[\dot{x}_4 - \frac{\partial f_4}{\partial x_1} |_{x^*} x_1\right] \Rightarrow x_4 = h_4(y, \dot{y}, \ddot{y}, y^{(3)}, y^{(4)}) \tag{69}$$

which signifies that the control input u is a differential function of the flat output of this robotic system. Therefore, all state variables and the control inputs of the PLI robot can be written as differential functions of the system's flat output and this confirms that the robotic system is differentially flat.

5.2. Design of a flatness-based controller for the PLI robot

Next, it will be shown that the differentially flat state-space model of the PLI robot can be written in the input-output linearized form and in the associated canonical Brunovsky form. In the second row of Eq. (65) one defines

$$\tilde{f}_2 = \frac{\partial f_2}{\partial x_1} |_{x^*} x_1 + \frac{\partial f_2}{\partial x_3} |_{x^*} x_3 \tag{70}$$

or equivalently

$$\begin{aligned} \tilde{f}_2 = & \frac{-(m_1 g h_1 + m_2 g h_{20}) sin(x_1) + m_2 g cos(x_1)}{m_1 h_1^2 + m_2 h_{20}^2} x_1 + \\ & + \frac{m_2 g cos(x_1)(m_1 h_1^2 + m_2 h_{20}^2) + [(m_1 g h_1 + m_2 g h_{20}) cos(x_1) + d_1 sin(x_1)](m_2 2 h_{20} l)}{(m_1 h_1^2 + m_2 h_{20}^2)^2} x_3 \end{aligned} \tag{71}$$

In the fourth row of the state-space model of Eq. (65) one defines

$$\tilde{f}_4 = \frac{\partial f_4}{\partial x_1} |_{x^*} x_1 \tag{72}$$

or equivalently

$$\tilde{f}_4 = \frac{1}{m_2 l^2}(m_2 g l cos(x_1)) x_1 \tag{73}$$

Next, successive differentiations of the flat output $y = x_1$ are performed until the control input u appears. It holds that

$$\begin{aligned} & \dot{x}_1 = x_2 \Rightarrow \ddot{x}_1 = \dot{x}_2 \Rightarrow \ddot{x}_1 = \tilde{f}_2 \\ & \Rightarrow x_1^{(3)} = \dot{\tilde{f}}_2 \end{aligned} \tag{74}$$

https://doi.org/10.1017/S026357472100148X Published online by Cambridge University Press

which in turn gives

$$x_1^{(3)} = \frac{-(m_1gh_1 + m_2gh_{20})cos(x_1)x_2 - m_2gsin(x_1)x_2}{m_1h_1^2 + m_2h_{20}^2}x_2 + \\ + \frac{-(m_1gh_1 + m_2gh_{20})sin(x_1) + m_2gcos(x_1)}{m_1h_1^2 + m_2h_{20}^2}x_2 + \\ + \frac{-m_2gsin(x_1)x_2(m_1h_1^2 + m_2h_{20}^2) + [(m_1gh_1 + m_2gh_{20})(- sin(x_1)x_2) + d_1cos(x_1)x_2](m_2 2h_{20}l)}{(m_1h_1^2 + m_2h_{20}^2)^2}x_3 + \\ + \frac{m_2gcos(x_1)(m_1h_1^2 + m_2h_{20}^2) + [(m_1gh_1 + m_2gh_{20})cos(x_1) + d_1sin(x_1)](m_2 2h_{20}l)}{(m_1h_1^2 + m_2h_{20}^2)^2}x_4 \tag{75}$$

Next, using Eq. (75) the following functions are defined

$$f_a(x_1, x_2) = \frac{-(m_1gh_1 + m_2gh_{20})cos(x_1)x_2 - m_2gsin(x_1)x_2}{m_1h_1^2 + m_2h_{20}^2} \tag{76}$$

$$f_b(x_1) = \frac{-(m_1gh_1 + m_2gh_{20})sin(x_1) + m_2gcos(x_1)}{m_1h_1^2 + m_2h_{20}^2} \tag{77}$$

$$f_c(x_1, x_2) = \frac{-m_2gsin(x_1)x_2(m_1h_1^2 + m_2h_{20}^2) + [(m_1gh_1 + m_2gh_{20})(- sin(x_1)x_2) + d_1cos(x_1)x_2](m_2 2h_{20}l)}{(m_1h_1^2 + m_2h_{20}^2)^2} \tag{78}$$

$$f_d(x_1) = \frac{m_2gcos(x_1)(m_1h_1^2 + m_2h_{20}^2) + [(m_1gh_1 + m_2gh_{20})cos(x_1) + d_1sin(x_1)](m_2 2h_{20}l)}{(m_1h_1^2 + m_2h_{20}^2)^2} \tag{79}$$

Besides, one computes the following time derivatives of functions $f_a(x_1, x_2), f_b(x_1), f_c(x_1, x_2)$ and $f_d(x_1)$

$$\dot{f}_a(x_1, x_2) = \frac{-(m_1gh_1 + m_2gh_{20})(- sin(x_1)x_2^2 + cos(x_1)\tilde{f}_2)) - m_2g(cos(x_1)x_2^2 + sin(x_1)\tilde{f}_2)}{m_1h_1^2 + m_2h_{20}^2} \tag{80}$$

$$\dot{f}_b(x_1, x_2) = \frac{-(m_1gh_1 + m_2gh_{20})cos(x_1)x_2 + m_2g(- sin(x_1)x_2)}{m_1h_1^2 + m_2h_{20}^2} \tag{81}$$

$$\dot{f}_c(x_1, x_2) = \frac{-m_2g(cos(x_1)x_2^2 + cos(x_1)\tilde{f}_2)(m_1h_1^2 + m_2h_{20}^2)}{(m_1h_1^2 + m_2h_{20}^2)^2} + \\ + \frac{[(m_1gh_1 + m_2gh_{20})(- cos(x_1)x_2^2 - sin(x_1)\tilde{f}_2) + d_1(- sin(x_1)x_2^2 + cos(x_1)\tilde{f}_2)](m_2 2h_{20}l)}{(m_1h_1^2 + m_2h_{20}^2)^2} \tag{82}$$

$$\dot{f}_d(x_1, x_2) = \frac{m_2g(- sin(x_1)x_2)(m_1h_1^2 + m_2h_{20}^2) + [(m_1gh_1 + m_2gh_{20})(- sin(x_1)x_2) + d_1(cos(x_1)x_2)](m_2 2h_{20}l)}{(m_1h_1^2 + m_2h_{20}^2)^2} \tag{83}$$

Consequently, one obtains

$$x_1^{(3)} = f_a(x_1, x_2)x_1 + f_b(x_1)x_2 + f_c(x_1, x_2)x_3 + f_d(x_1)x_4 \tag{84}$$

By differentiating once again with respect to time one obtains

$$x_1^{(4)} = \dot{f}_a(x_1, x_2)x_1 + f_a(x_1, x_2)x_2 + \dot{f}_b(x_1)x_2 + f_b(x_1)\tilde{f}_2 + \\ + \dot{f}_c(x_1, x_2)x_3 + f_c(x_1, x_2)x_4 + \dot{f}_d(x_1)x_4 + f_d(x_1)[\tilde{f}_4 + g_4u] \tag{85}$$

https://doi.org/10.1017/S026357472100148X Published online by Cambridge University Press

The previous equation is rewritten in the concise form

$$x_1^{(4)} = \bar{f} + \bar{g}u \tag{86}$$

where functions $\bar{f}$ and $\bar{g}$ are differential functions of the flat output of the robotic system and are defined as

$$\begin{gathered}\bar{f} = \left\{\dot{f}_a(x_1, x_2)x_1 + f_a(x_1, x_2)x_2 + \dot{f}_b(x_1)x_2 + f_b(x_1)\tilde{f}_2 + \right. \\ \left. + \dot{f}_c(x_1, x_2)x_3 + f_c(x_1, x_2)x_4 + \dot{f}_d(x_1)x_4 + f_d(x_1)\tilde{f}_4\right\} \\ \bar{g} = f_d(x_1)g_4\end{gathered} \tag{87}$$

Next, the cumulative control input $v = \bar{f} + \bar{g}u$ is defined. It holds that

$$x_1^{(4)} = v \tag{88}$$

while one can also arrive at the following canonical Brunovsky form

$$\begin{pmatrix} \dot{y} \\ \ddot{y} \\ y^{(3)} \\ y^{(4)} \end{pmatrix} = \begin{pmatrix} 0 & 1 & 0 & 0 \\ 0 & 0 & 1 & 0 \\ 0 & 0 & 0 & 1 \\ 0 & 0 & 0 & 0 \end{pmatrix} \begin{pmatrix} y \\ \dot{y} \\ \ddot{y} \\ y^{(3)} \end{pmatrix} + \begin{pmatrix} 0 \\ 0 \\ 0 \\ 1 \end{pmatrix} v \tag{89}$$

The stabilizing feedback control is

$$v = x_{1,d}^{(4)} - k_1\left(x_1^{(3)} - x_{1,d}^{(3)}\right) - k_2(\ddot{x}_1 - \ddot{x}_{1,d}) - k_3(\dot{x}_1 - \dot{x}_{1,d}) - k_4(x_1 - x_{1,d}) \tag{90}$$

which results into the following tracking error dynamics

$$\begin{gathered}\left(x^{(4)} - x_{1,d}^{(4)}\right) + k_1\left(x_1^3 - x_{1,d}^{(3)}\right) + k_2(\ddot{x}_1 - \ddot{x}_{1,d}) + k_3(\dot{x}_1 - \dot{x}_{1,d}) + k_4(x_1 - x_{1,d}) = 0 \Rightarrow \\ e^{(4)} + k_1 e^{(3)} + k_2\ddot{e} + k_3\dot{e} + k_4 e = 0\end{gathered} \tag{91}$$

The associated characteristic polynomial is

$$p(s) = s^4 + k_1 s^2 + k_2 s^2 + k_3 s + k_4 \tag{92}$$

The stabilizing feedback control gains k_1, k_2, k_3, k_4 are selected according to the requirement the above noted characteristic polynomial to be Hurwitz stable, that is to have poles in the left complex semiplane. The state-estimation problem for the system of Eq. (89) is solved using Kalman filtering. The Kalman filter's recursion followed by the previously defined differential flatness transformations in Eqs. (66), (67), and (68) is known as derivative-free nonlinear Kalman filter [25, 37].

The flatness-based control input which is applied to the real nonlinear dynamics of the PLI robot is

$$v = \bar{f} + \bar{g}u \Rightarrow u = \bar{g}^{-1}[v - \bar{f}] \tag{93}$$

Remark 1: The comparison between nonlinear optimal control and flatness-based control has shown that (i) nonlinear optimal control does not require new state variables definitions and transformation of the state-space representation of the PLI robot, whereas flatness-based control is based on diffeomorphisms that is changes of the state-variables of the robot's model, (ii) nonlinear optimal control, although being based on an approximate linearization concept achieves comparable tracking performance to the flatness-based control approach, which is based on exact modelling of the robot's dynamics and a global linearization transformation, and (iii) nonlinear optimal control is applied directly on the initial nonlinear state-space model of the PLI robot, whereas flatness-based control computes control inputs for the linearized equivalent model of the robot and next uses an inverse transformation to obtain the control inputs which should be applied to the real dynamics of the PLI robot. Thus, in the first case, singularities that are related to the inverse transformations are avoided. Despite its conceptual simplicity, the nonlinear optimal control approach is reliable. Besides, it is the only method that assures optimality with respect to the minimization of the energy dissipation by the robot's actuators.

https://doi.org/10.1017/S026357472100148X Published online by Cambridge University Press

6. Design of a Sliding-Mode Controller for the PLI Robot

After input–output linearization, and as shown in Eq. (86), the dynamic model of the underactuated power-lies inspection robot is written as

$$x_1^{(4)} = \bar{f}(x) + \bar{g}(x)u \tag{94}$$

where the term $\bar{f}$ is considered to vary within the uncertainty regions $[f - \bar{f}] \leq \Delta\bar{f}$. The output tracking error for the robotic system is defined as $e_1 = x_1 - x_1^d$. The sliding surface for the PLI robot is defined as

$$s = e_1^{(3)} + \lambda_1\ddot{e}_1 + \lambda_2\dot{e}_1 + \lambda_3 \tag{95}$$

Provided that the polynomial $p(e) = e^3 + \lambda_1 e^2 + \lambda_2 e + \lambda_3$ is Hurwitz stable, the condition about the elimination of the tracking error comes from $lim_{t\to\infty} s = 0$. The convergence of the sliding surface to 0 is ensured, if the following condition holds for the Lyapunov-like function of the system

$$\frac{1}{2}\frac{d}{dt}s^2 \leq -\eta|s| \text{ for } \eta > 0 \tag{96}$$

The sliding-mode controller for the PLI robot consists of the equivalent control part and the switching control part

$$u = u_{eq} + u_{sw} \tag{97}$$

Actually, the equivalent controller is computed from the condition $\dot{s} = 0$

$$\begin{gathered}
\dot{s} = 0 \Rightarrow e_1^{(4)} + \lambda_1 e_1^{(3)} + \lambda_2\ddot{e}_1 + \lambda_3 e_1 = 0 \Rightarrow \\
x^{(4)} - x_d^{(4)} + \lambda_1 e_1^{(3)} + \lambda_2\ddot{e}_1 + \lambda_3 e_1 = 0 \Rightarrow \\
\bar{f}(x) + \bar{g}(x)u - x_d^{(4)} + \lambda_1\left(x_1^{(3)} - x_{1,d}^{(3)}\right) + \lambda_2(\ddot{x}_1 - \ddot{x}_{1,d}) + \lambda_3(\dot{x}_1 - \dot{x}_{1,d}) = 0 \Rightarrow \\
u_{eq} = \frac{1}{\bar{g}(x)}\left[x_d^{(4)} - \bar{f}(x) - \lambda_1\left(x_1^{(3)} - x_{1,d}^{(3)}\right) - \lambda_2(\ddot{x}_1 - \ddot{x}_{1,d}) - \lambda_3(\dot{x}_1 - \dot{x}_{1,d})\right]
\end{gathered} \tag{98}$$

The switching control law is taken to be

$$u_{sw} = -\frac{1}{\bar{g}(x)}K_1 sgn(s) \tag{99}$$

with gain $K_1 > 0$. Thus, the aggregate sliding-mode control law is given by

$$\begin{gathered}
u = u_{eq} + u_{sw} \Rightarrow \\
u = \frac{1}{\bar{g}(x)}\left[x_d^{(4)} - \bar{f}(x) - \lambda_1\left(x_1^{(3)} - x_{1,d}^{(3)}\right) - \lambda_2(\ddot{x}_1 - \ddot{x}_{1,d}) - \lambda_3(\dot{x}_1 - \dot{x}_{1,d}) - K_1 sgn(s)\right]
\end{gathered} \tag{100}$$

Next, it is confirmed that under the sliding-mode control law of Eq. (100) the stability condition of Eq. (96)) holds. By substituting the control law of Eq. (100) into Eq. (94), one gets

$$\begin{gathered}
x^{(4)} = \bar{f}(x) + \bar{g}(x)u \Rightarrow \\
x^{(4)} = \bar{f}(x) + \bar{g}(x)\frac{1}{\bar{g}(x)}\left[x_d^{(4)} - \hat{\bar{f}}(x) - \lambda_1\left(x_1^{(3)} - x_{1,d}^{(3)}\right) - \lambda_2(\ddot{x}_1 - \ddot{x}_{1,d}) - \lambda_3(\dot{x}_1 - \dot{x}_{1,d}) - K_1 sgn(s)\right]
\end{gathered} \tag{101}$$

By performing intermediate operations one obtains

$$\begin{gathered}
x^{(4)} = \bar{f}(x) + x_{1,d}^{(4)} - \hat{\bar{f}}(x) - \lambda_1\left(x_1^{(3)} - x_{1,d}^{(3)}\right) - \lambda_2(\ddot{x}_1 - \ddot{x}_{1,d}) - \lambda_3(\dot{x}_1 - \dot{x}_{1,d})] - K_1 sgn(s) \Rightarrow \\
x^{(4)} - x_{1,d}^{(4)} + \lambda_1\left(x_1^{(3)} - x_{1,d}^{(3)}\right) + \lambda_2(\ddot{x}_1 - \ddot{x}_{1,d}) + \lambda_3(\dot{x}_1 - \dot{x}_{1,d})] = \left[\bar{f}(x) - \hat{\bar{f}}(x)\right] - K_1 sgn(s)
\end{gathered} \tag{102}$$

Next, using that $|\bar{f} - \hat{\bar{f}}| \leq \Delta\bar{f}$ Eq. (102) gives

$$\begin{gathered}
e^{(4)} + \lambda_1 e^{(3)} + \lambda_2\ddot{e} + \lambda_3\dot{e} \leq \Delta\bar{f} - K_1 sgn(s) \Rightarrow \\
\dot{s} \leq \Delta\bar{f} - K_1 sgn(s)
\end{gathered} \tag{103}$$

https://doi.org/10.1017/S026357472100148X Published online by Cambridge University Press

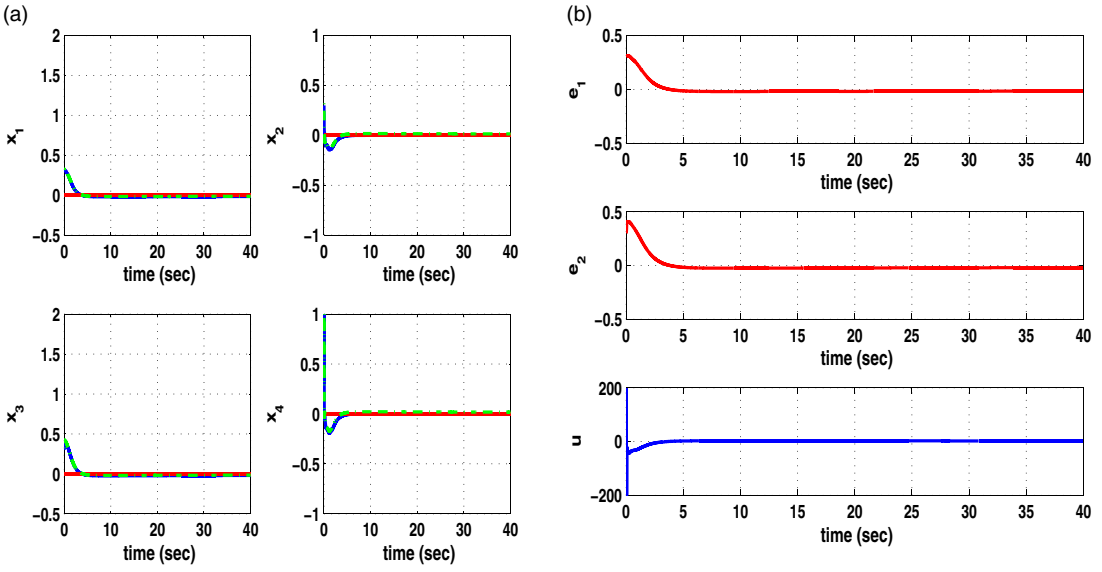


Figure 4. *Nonlinear optimal control of the power-line inspection robot when tracking setpoint 1 (a) state variables x_i $i=1,\cdots,4$ (blue lines), their estimated values (green lines) and the associated reference setpoints (red lines), (b) tracking errors e_1 (state variable x_1) and e_2 (state variable x_3) and control input u of the power-line inspection robot.*

Thus, by substituting Eq. (103) into Eq. (96), one gets

$$\begin{aligned} &\frac{1}{2}\frac{d}{dt}s^2 \leq -\eta|s| \Rightarrow s\dot{s} \leq -\eta|s| \Rightarrow \\ &s\left[\Delta\bar{f} - K_1 sgn(s)\right] \leq -\eta|s| \Rightarrow \\ &s\Delta\bar{f} - sK_1 sgn(s) \leq -\eta|s| \end{aligned} \tag{104}$$

By selecting the gain of the switching control term to be $K_1 = \Delta\bar{f} + \eta$,

$$\begin{aligned} &s\Delta\bar{f} - |s|\Delta\bar{f} - \eta|s| \leq -\eta|s| \Rightarrow \\ &s\Delta\bar{f} \leq |s|\Delta\bar{f} \Rightarrow s \leq |s| \end{aligned} \tag{105}$$

The final relation $s \leq |s|$ holds always. This means that the proposed sliding-mode control method assures global stability for the control input of the PLI robot.

7. Simulation Tests

7.1. Results on nonlinear optimal control of the PLI robot

The tracking performance of the proposed nonlinear optimal (H-infinity) control method for PLI robots was tested through simulation experiments. Indicative values for the parameters of the model of the robotic mechanism are $l = 0.5$ m, $d_1 = 0.5$ m, $g = 10\,\text{m/sec}^2$, $m_1 = 63$ Kgr, $m_2 = 27$ Kgr, $h_1 = 0.18$ m, and $h_{20} = 0.42$ m [1]. The sampling period was $T_s = 0.01$ sec. The obtained results are given in Figs. 4, 5, 6, 7, 8, and 9. The state variables of the PLI robot are printed in blue color, the estimated state variables that were provided by the H-infinity Kalman filter are marked in green, while the related setpoints are plotted in red. The measurement units of angles θ_1 and θ_2 are in rad, while the measurement units of the angular velocities $\dot{\theta}_1$ and $\dot{\theta}_2$ are in rad/sec. The control input u is a torque measured in Ntm. It can be noticed that the tracking error for all state variables of the robotic mechanism has been eliminated, while the transient performance of the control loop was good. Actually, there were neither abrupt variations of

https://doi.org/10.1017/S026357472100148X Published online by Cambridge University Press

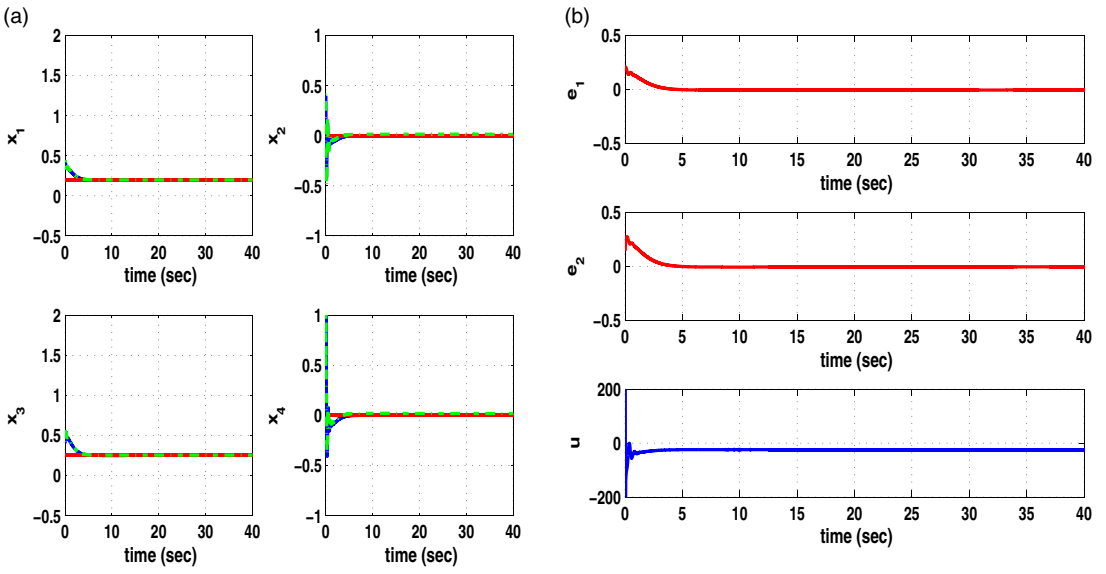


Figure 5. *Nonlinear optimal control of the power-line inspection robot when tracking setpoint 2 (a) state variables x_i $i = 1, \cdots, 4$ (blue lines), their estimated values (green lines) and the associated reference setpoints (red lines), (b) tracking errors e_1 (state variable x_1) and e_2 (state variable x_3) and control input u of the power-line inspection robot.*

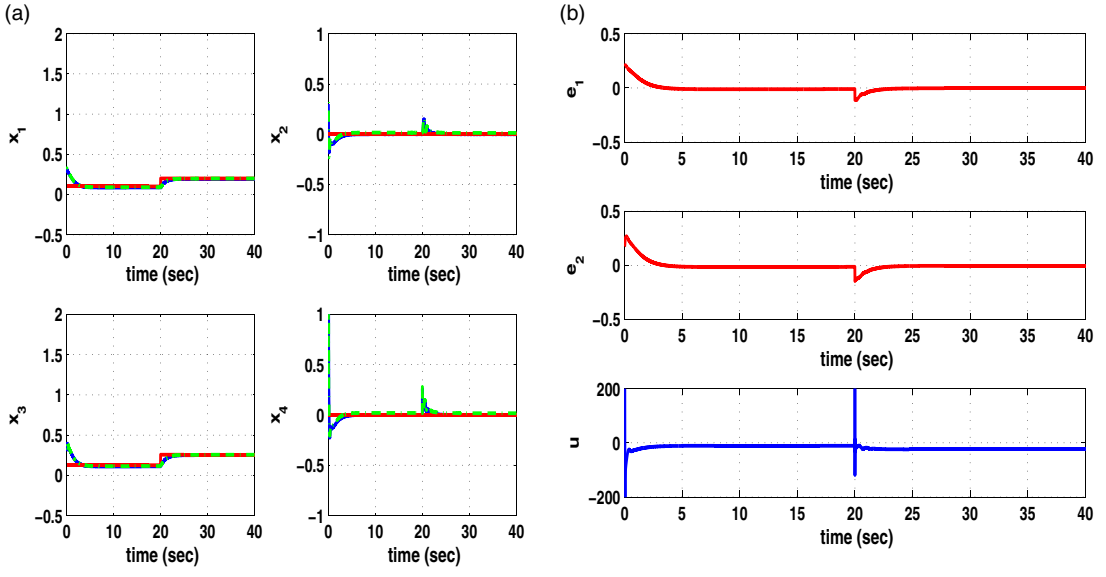


Figure 6. *Nonlinear optimal control of the power-line inspection robot when tracking setpoint 3 (a) state variables x_i $i = 1, \cdots, 4$ (blue lines), their estimated values (green lines) and the associated reference setpoints (red lines), (b) tracking errors e_1 (state variable x_1) and e_2 (state variable x_3) and control input u of the power-line inspection robot.*

the state variables nor excessive values of the control inputs. The transient performance of the control loop depends on the selection of values for parameters r, ρ, and Q which appear in the algebraic Riccati equation given in Eq. (49). The smallest value of ρ for which one can obtain a valid solution of the previously noted Riccati equation is the one that provides the control loop with maximum robustness.

https://doi.org/10.1017/S026357472100148X Published online by Cambridge University Press

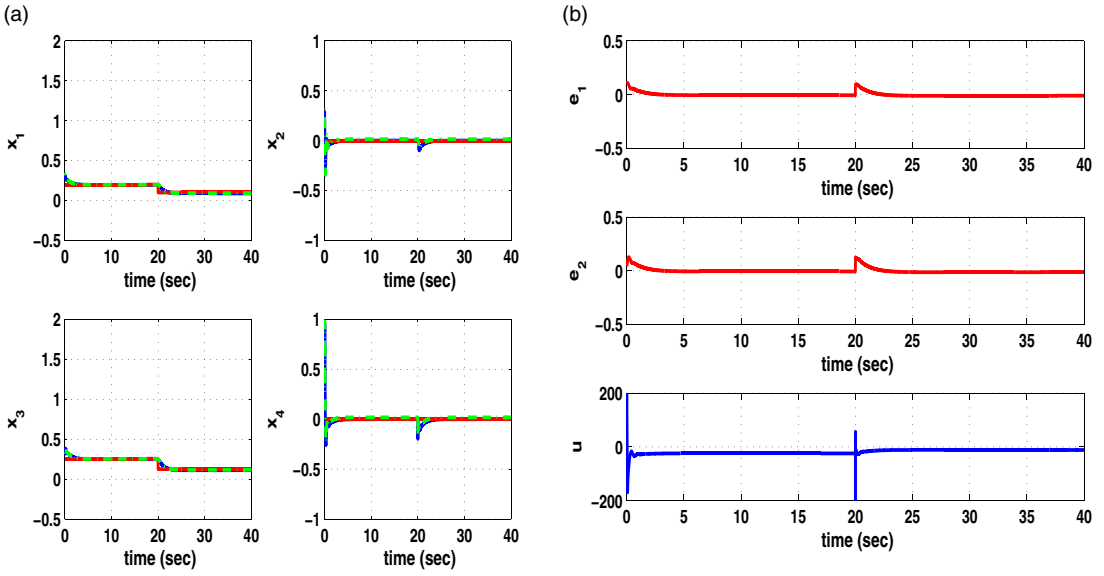


Figure 7. *Nonlinear optimal control of the power-line inspection robot when tracking setpoint 4 (a) state variables x_i $i = 1, \cdots, 4$ (blue lines), their estimated values (green lines) and the associated reference setpoints (red lines), (b) tracking errors e_1 (state variable x_1) and e_2 (state variable x_3) and control input u of the power-line inspection robot.*

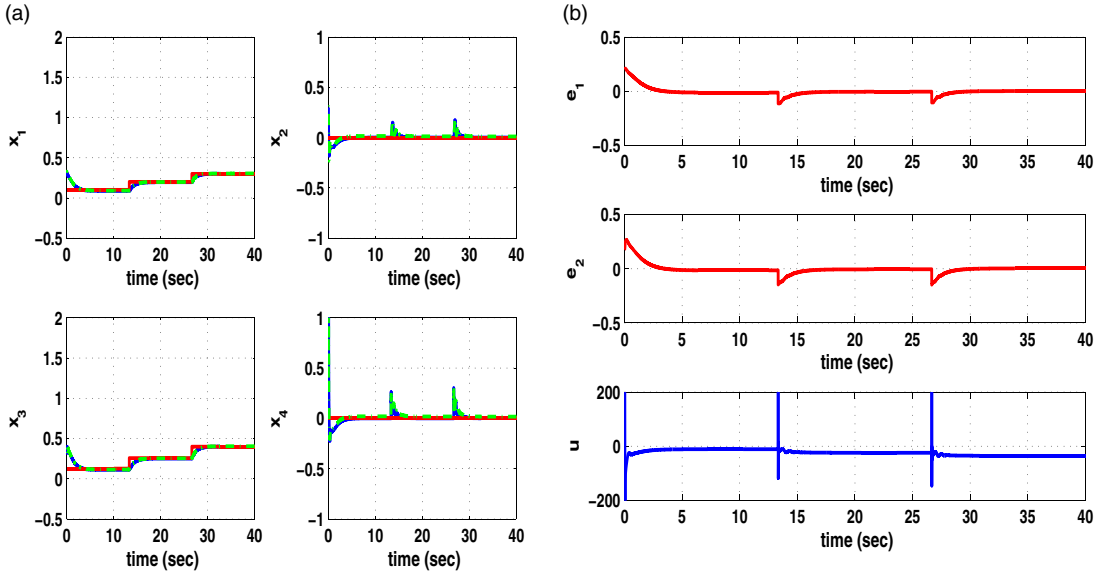


Figure 8. *Nonlinear optimal control of the PLI robot when tracking setpoint 5 (a) state variables x_i $i = 1, \cdots, 4$ (blue lines), their estimated values (green lines) and the associated reference setpoints (red lines), (b) tracking errors e_1 (state variable x_1) and e_2 (state variable x_3) and control input u of the PLI robot.*

To elaborate on the tracking performance and on the robustness of the proposed nonlinear optimal control method for the PLI robot, the following tables are given: (i) Table I that provides information about the accuracy of tracking of the reference setpoints by the state variables of the PLI robot under an exact model, (ii) Table II that provides information about the robustness of the control method to

https://doi.org/10.1017/S026357472100148X Published online by Cambridge University Press

Table I. *Nonlinear optimal control RMSE for the PLI robot without disturbances.*

	$RMSE_{x_1}$	$RMSE_{x_2}$	$RMSE_{x_3}$	$RMSE_{x_4}$
setpoint_1	$0.7807 \cdot 10^{-3}$	$0.0027 \cdot 10^{-3}$	$0.9760 \cdot 10^{-3}$	$0.0089 \cdot 10^{-3}$
setpoint_2	$0.1825 \cdot 10^{-3}$	$0.0030 \cdot 10^{-3}$	$0.2451 \cdot 10^{-3}$	$0.0053 \cdot 10^{-3}$
setpoint_3	$0.1665 \cdot 10^{-3}$	$0.0134 \cdot 10^{-3}$	$0.2225 \cdot 10^{-3}$	$0.0130 \cdot 10^{-3}$
setpoint_4	$0.4803 \cdot 10^{-3}$	$0.0165 \cdot 10^{-3}$	$0.6099 \cdot 10^{-3}$	$0.0206 \cdot 10^{-3}$
setpoint_5	$0.2124 \cdot 10^{-3}$	$0.2490 \cdot 10^{-3}$	$0.3153 \cdot 10^{-3}$	$0.3693 \cdot 10^{-3}$
setpoint_6	$0.3813 \cdot 10^{-3}$	$0.3581 \cdot 10^{-3}$	$0.4856 \cdot 10^{-3}$	$0.4611 \cdot 10^{-3}$

Table II. *Nonlinear optimal control RMSE for the PLI robot under disturbances.*

$\Delta a\%$	$RMSE_{x_1}$	$RMSE_{x_2}$	$RMSE_{x_3}$	$RMSE_{x_4}$
0%	$0.1810 \cdot 10^{-3}$	$0.0054 \cdot 10^{-3}$	$0.2431 \cdot 10^{-3}$	$0.0063 \cdot 10^{-3}$
10%	$0.1843 \cdot 10^{-3}$	$0.0054 \cdot 10^{-3}$	$0.2482 \cdot 10^{-3}$	$0.0065 \cdot 10^{-3}$
20%	$0.1909 \cdot 10^{-3}$	$0.0041 \cdot 10^{-3}$	$0.2564 \cdot 10^{-3}$	$0.0051 \cdot 10^{-3}$
30%	$0.1980 \cdot 10^{-3}$	$0.0052 \cdot 10^{-3}$	$0.2629 \cdot 10^{-3}$	$0.0066 \cdot 10^{-3}$
40%	$0.2047 \cdot 10^{-3}$	$0.0050 \cdot 10^{-3}$	$0.2749 \cdot 10^{-3}$	$0.0064 \cdot 10^{-3}$
50%	$0.2222 \cdot 10^{-3}$	$0.0046 \cdot 10^{-3}$	$0.2984 \cdot 10^{-3}$	$0.0057 \cdot 10^{-3}$
60%	$0.2393 \cdot 10^{-3}$	$0.0051 \cdot 10^{-3}$	$0.3212 \cdot 10^{-3}$	$0.0069 \cdot 10^{-3}$

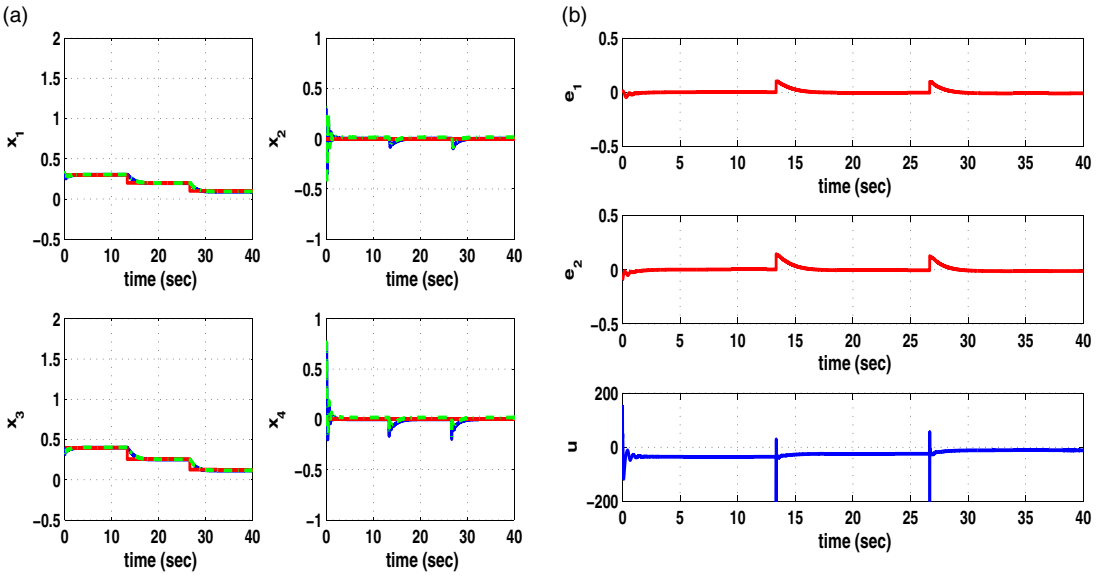


Figure 9. *Nonlinear optimal control of the PLI robot when tracking setpoint 6 (a) state variables x_i $i = 1, \cdots, 4$ (blue lines), their estimated values (green lines) and the associated reference setpoints (red lines), (b) tracking errors e_1 (state variable x_1) and e_2 (state variable x_3) and control input u of the PLI robot.*

parametric changes in the model of the PLI robot (change in drift term f_2 in the second row of the state-space model, up to 60%). Equivalent results, showing robustness of the control loop have been obtained for changes of the counter-weight mass m_2 of up to 20%. (iii) Table III which provides information about the precision in state variables' estimation that is achieved by the H-infinity Kalman filter, (iv) Table IV which provides the tracking precision of the PLI robot under variable levels (variance) of sensors' measurement noise.

https://doi.org/10.1017/S026357472100148X Published online by Cambridge University Press

Table III. *Nonlinear optimal control RMSE for the estimation performed by the H-infinity KF.*

	$RMSE_{x_1}$	$RMSE_{x_2}$	$RMSE_{x_3}$	$RMSE_{x_4}$
setpoint_1	$0.0215 \cdot 10^{-3}$	$0.7181 \cdot 10^{-3}$	$0.0253 \cdot 10^{-3}$	$0.8414 \cdot 10^{-3}$
setpoint_2	$0.0184 \cdot 10^{-3}$	$0.0162 \cdot 10^{-3}$	$0.0264 \cdot 10^{-3}$	$0.8042 \cdot 10^{-3}$
setpoint_3	$0.0179 \cdot 10^{-3}$	$0.6022 \cdot 10^{-3}$	$0.0233 \cdot 10^{-3}$	$0.7778 \cdot 10^{-3}$
setpoint_4	$0.0205 \cdot 10^{-3}$	$0.6841 \cdot 10^{-3}$	$0.0251 \cdot 10^{-3}$	$0.8377 \cdot 10^{-3}$
setpoint_5	$0.0161 \cdot 10^{-3}$	$0.5258 \cdot 10^{-3}$	$0.0232 \cdot 10^{-3}$	$0.7606 \cdot 10^{-3}$
setpoint_6	$0.0197 \cdot 10^{-3}$	$0.6634 \cdot 10^{-3}$	$0.0252 \cdot 10^{-3}$	$0.8392 \cdot 10^{-3}$

Table IV. *Nonlinear optimal control RMSE for the PLI robot under variable noise levels.*

Noise level	$RMSE_{x_1}$	$RMSE_{x_2}$	$RMSE_{x_3}$	$RMSE_{x_4}$
$\sigma_1 = 0.05$	$0.1123 \cdot 10^{-3}$	$0.3056 \cdot 10^{-3}$	$0.1393 \cdot 10^{-3}$	$0.3231 \cdot 10^{-3}$
$\sigma_2 = 0.06$	$0.0905 \cdot 10^{-3}$	$0.2091 \cdot 10^{-3}$	$0.1183 \cdot 10^{-3}$	$0.2118 \cdot 10^{-3}$
$\sigma_3 = 0.07$	$0.1529 \cdot 10^{-3}$	$0.2439 \cdot 10^{-3}$	$0.2058 \cdot 10^{-3}$	$0.3499 \cdot 10^{-3}$
$\sigma_4 = 0.08$	$0.2563 \cdot 10^{-3}$	$0.4174 \cdot 10^{-3}$	$0.3368 \cdot 10^{-3}$	$0.4697 \cdot 10^{-3}$
$\sigma_5 = 0.09$	$0.1658 \cdot 10^{-3}$	$0.3768 \cdot 10^{-3}$	$0.2146 \cdot 10^{-3}$	$0.3900 \cdot 10^{-3}$
$\sigma_6 = 0.10$	$0.1633 \cdot 10^{-3}$	$0.3602 \cdot 10^{-3}$	$0.2115 \cdot 10^{-3}$	$0.4133 \cdot 10^{-3}$

Comparing to other nonlinear control methods for the model of the PLI robot, the proposed nonlinear optimal (H-infinity) control approach exhibits specific advantages (i) unlike global linearization-based control methods (such as Lie algebra-based control or differential flatness theory-based control), the article's optimal control scheme does not need complicated state variables transformations (diffeomorphisms). Besides, in the article's approach the control inputs are applied directly on the initial nonlinear state-space model of the PLI robot and not on its linearized equivalent description. Thus, the inverse transformations and the related singularity problems that may appear in global linearization-based control methods can be avoided. (ii) unlike popular approaches to optimal control met in industry, such as Model Predictive Control (MPC) and Nonlinear Model Predictive Control (NMPC) the stability and convergence of the article's nonlinear optimal control scheme is assured. MPC is a linear control method and its use in the nonlinear dynamic model of the PLI robot will result into loss of stability. Besides, the convergence to an optimum for NMPC is dependent on initialization and parameter values selection and in general cannot be ascertained. (iii) unlike sliding-mode control and backstepping control, the application of the article's control method does not require the state-space description of the system to be found in a specific form. In the case of sliding-mode control, one has to define the sliding surface however there is no systematic procedure about this unless the system is found in the input-output linearized (canonical) form. In the case of backstepping control the system has to be found in the backstepping integral (triangular) form. For the state-space model of the PLI robot, none of the above two conditions holds, therefore the use of the article's nonlinear optimal control approach provides the only feasible solution, (iv) unlike PID control the article's control method is of proven global stability, assures reliable functioning of the PLI robot at all changes of operating points and does not involve any heuristics in the selection of the controller's gains, (v) unlike multiple models-based control, the article's control method is computationally more efficient because it performs linearization only around one time-varying setpoint, and involves the solution of only one Riccati equation.

7.2. Results on flatness-based control of the PLI robot

Control of the PLI robot was also performed by applying differential flatness theory. The sampling period was $T_s = 0.01$ sec. The input-output linearized state-space model of the PLI robot has been written in the

https://doi.org/10.1017/S026357472100148X Published online by Cambridge University Press

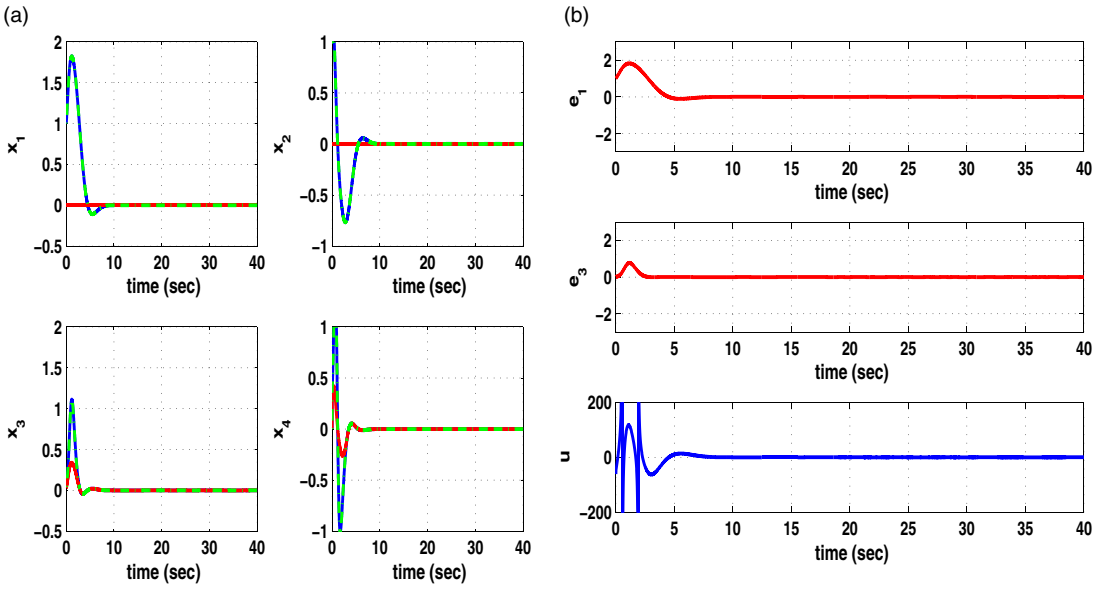


Figure 10. *Flatness-based control of the PLI robot when tracking setpoint 1: (a) state variables x_i $i = 1, \cdots, 4$ (blue lines), their estimated values (green lines) and the associated reference setpoints (red lines), (b) tracking errors e_1 (state variable x_1) and e_2 (state variable x_3) and control input u of the PLI robot.*

canonical Brunvosky form. The design of a stabilzing feedback controller has been based on the pole-placement (eigenvalues assignment) technique) that was described in Section 5. The measurable state variable was the turn angle $x_1 = \theta_1$ of the first joint of the robot. State estimation has been performed with the use of Kalman filtering. This filtering approach is also known as Derivative-free nonlinear Kalman filter (DKF). It consists of the Kalman filter's recursion being applied to the linearized state-space description of the PLI robot and is followed by inverse transformations which provide finally the state estimates of the initial nonlinear model of the PLI robot [34]. The obtained results are shown in Figs. 10, 11, 12, 13, 14 and 15. It can be noticed that the differential flatness theory-based control method had also satisfactory performance. The tracking accuracy of the flatness-based control scheme was at the same order of the one achieved by the above-noted nonlinear optimal control scheme (this accuracy is dependent also on the selection of the feedback control gains).

7.3. Results on sliding-mode control of the PLI robot

Control of the PLI robot was also performed by applying sliding-mode control. The sampling period was again $T_s = 0.01$ sec. The input-output linearized state-space model of the PLI robot has been written in the canonical Brunvosky form. The design of the sliding-mode control has been based on the technique that was described in Section 6. The measurable state variable was the turn angle $x_1 = \theta_1$ of the first joint of the robot. State estimation has been performed with the use of Kalman filtering as in the case of flatness-based control [34]. The obtained results are shown in Figs. 16, 17, 18, 19, 20 and 21. It can be noticed that sliding-mode control had also satisfactory performance. The tracking accuracy of the sliding-mode control scheme was at the same order of the one achieved by the above-noted nonlinear optimal control scheme. To limit the variations of the control inputs and to avoid the appearance of chattering in the control signal the switching control term based on a sign function of the sliding surface s was substituted by a saturation function.

https://doi.org/10.1017/S026357472100148X Published online by Cambridge University Press

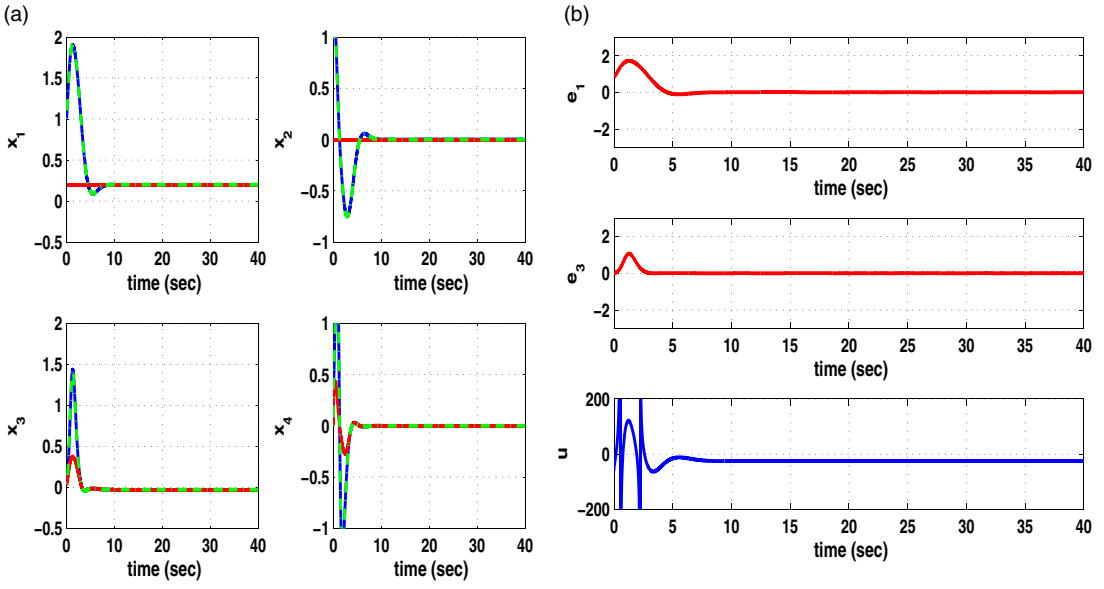


Figure 11. *Flatness-based control of the PLI robot when tracking setpoint 2: (a) state variables x_i $i = 1, \cdots, 4$ (blue lines), their estimated values (green lines) and the associated reference setpoints (red lines), (b) tracking errors e_1 (state variable x_1) and e_2 (state variable x_3) and control input u of the PLI robot.*

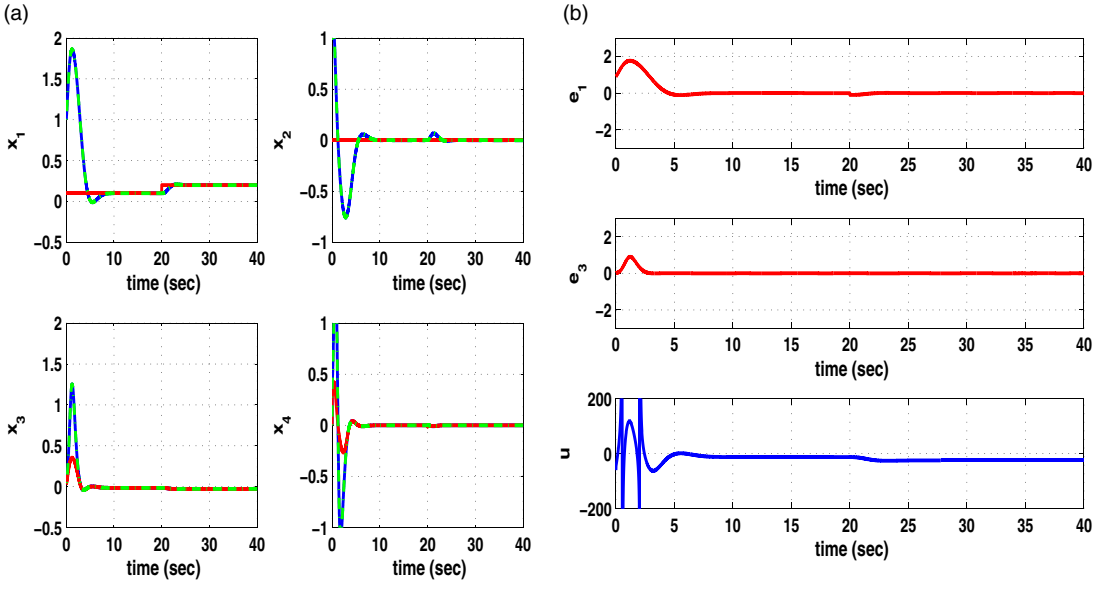


Figure 12. *Flatness-based control of the PLI robot when tracking setpoint 3: (a) state variables x_i $i = 1, \cdots, 4$ (blue lines), their estimated values (green lines) and the associated reference setpoints (red lines), (b) tracking errors e_1 (state variable x_1) and e_2 (state variable x_3) and control input u of the PLI robot.*

https://doi.org/10.1017/S026357472100148X Published online by Cambridge University Press

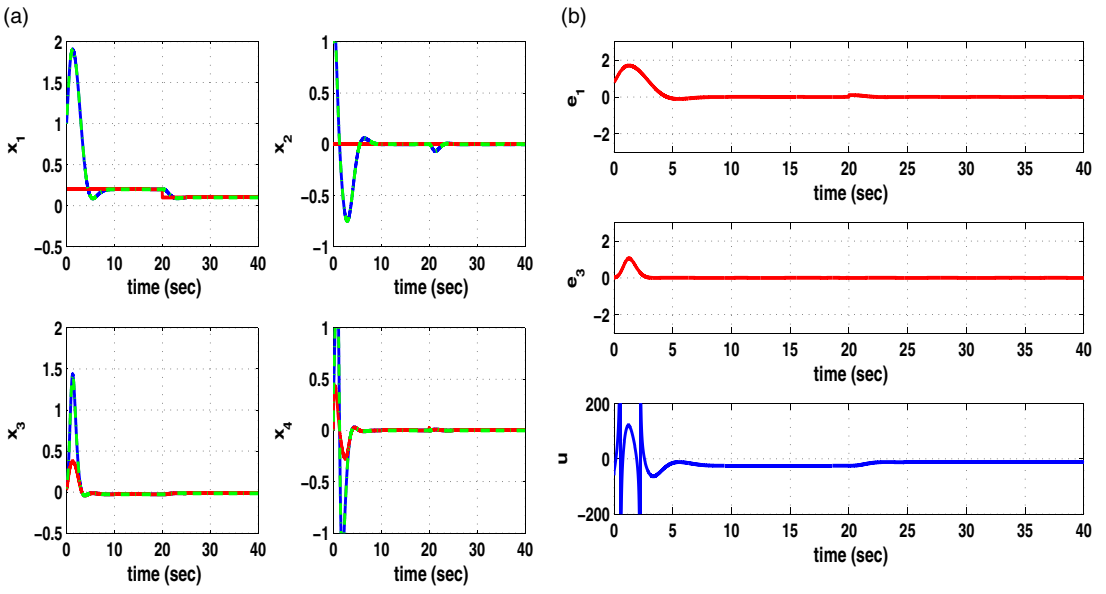


Figure 13. *Flatness-based control of the PLI robot when tracking setpoint 4: (a) state variables x_i $i = 1, \cdots, 4$ (blue lines), their estimated values (green lines) and the associated reference setpoints (red lines), (b) tracking errors e_1 (state variable x_1) and e_2 (state variable x_3) and control input u of the PLI robot.*

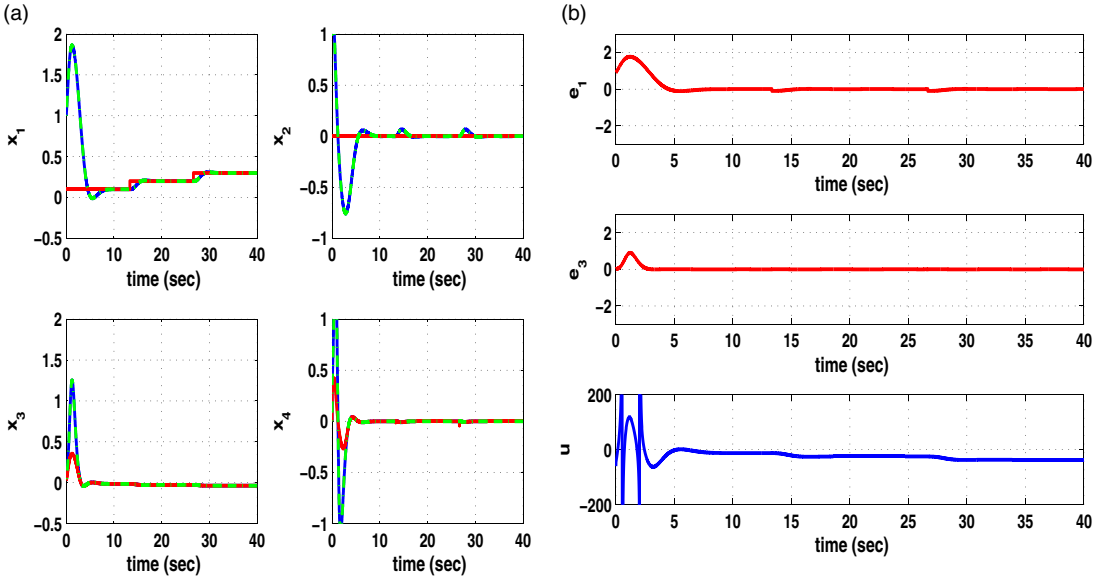


Figure 14. *Flatness-based control of the PLI robot when tracking setpoint 5: (a) state variables x_i $i = 1, \cdots, 4$ (blue lines), their estimated values (green lines) and the associated reference setpoints (red lines), (b) tracking errors e_1 (state variable x_1) and e_2 (state variable x_3) and control input u of the PLI robot.*

https://doi.org/10.1017/S026357472100148X Published online by Cambridge University Press

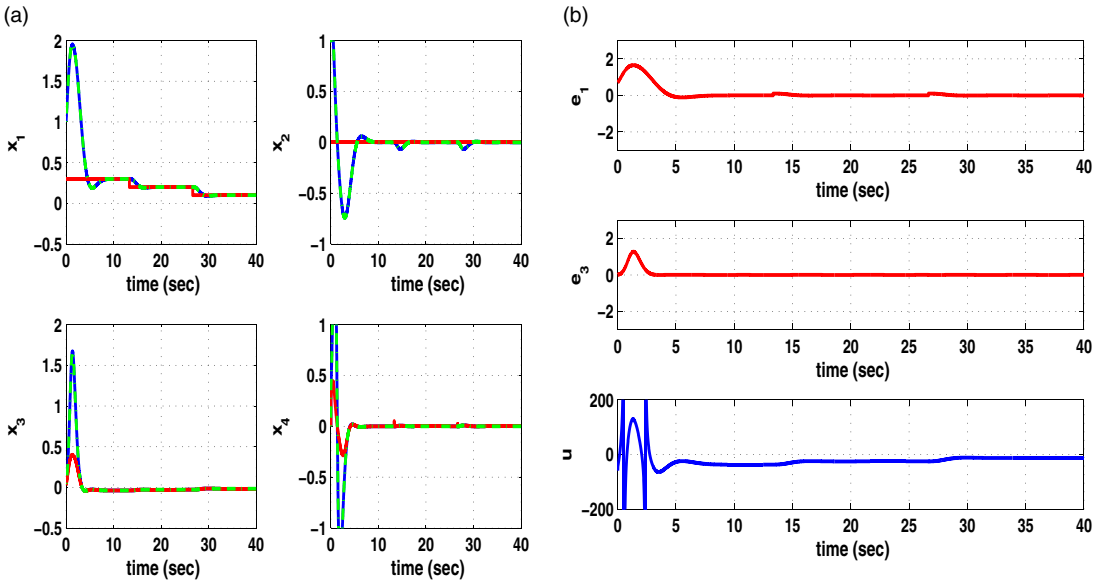


Figure 15. *Flatness-based control of the PLI robot when tracking setpoint 6: (a) state variables x_i $i = 1, \cdots, 4$ (blue lines), their estimated values (green lines) and the associated reference setpoints (red lines), (b) tracking errors e_1 (state variable x_1) and e_2 (state variable x_3) and control input u of the PLI robot.*

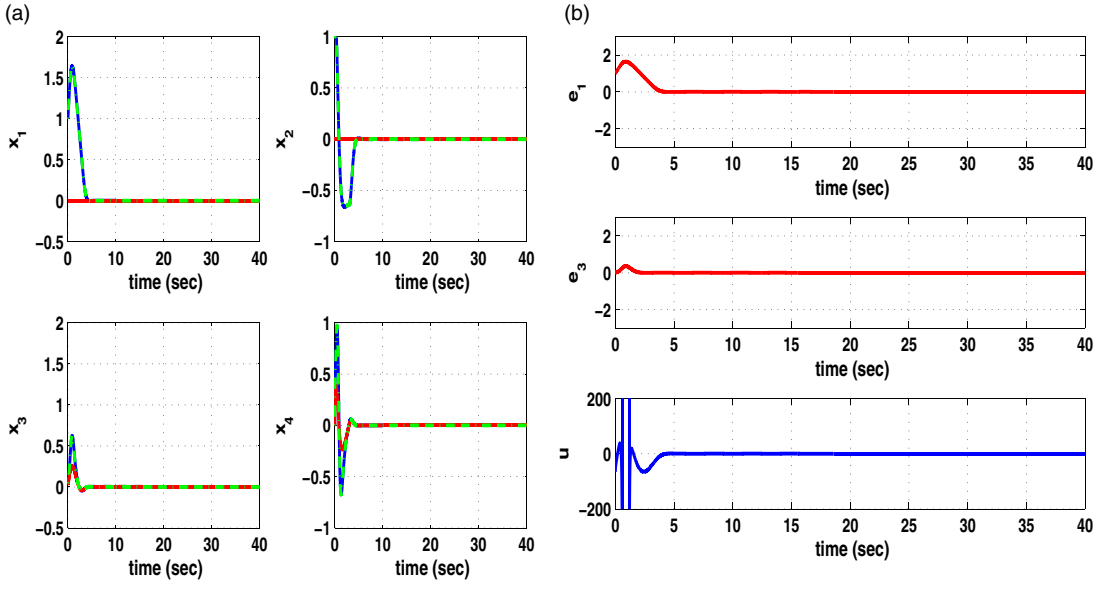


Figure 16. *Sliding-mode control of the PLI robot when tracking setpoint 1: (a) state variables x_i $i = 1, \cdots, 4$ (blue lines), their estimated values (green lines) and the associated reference setpoints (red lines), (b) tracking errors e_1 (state variable x_1) and e_2 (state variable x_3) and control input u of the PLI robot.*

https://doi.org/10.1017/S026357472100148X Published online by Cambridge University Press

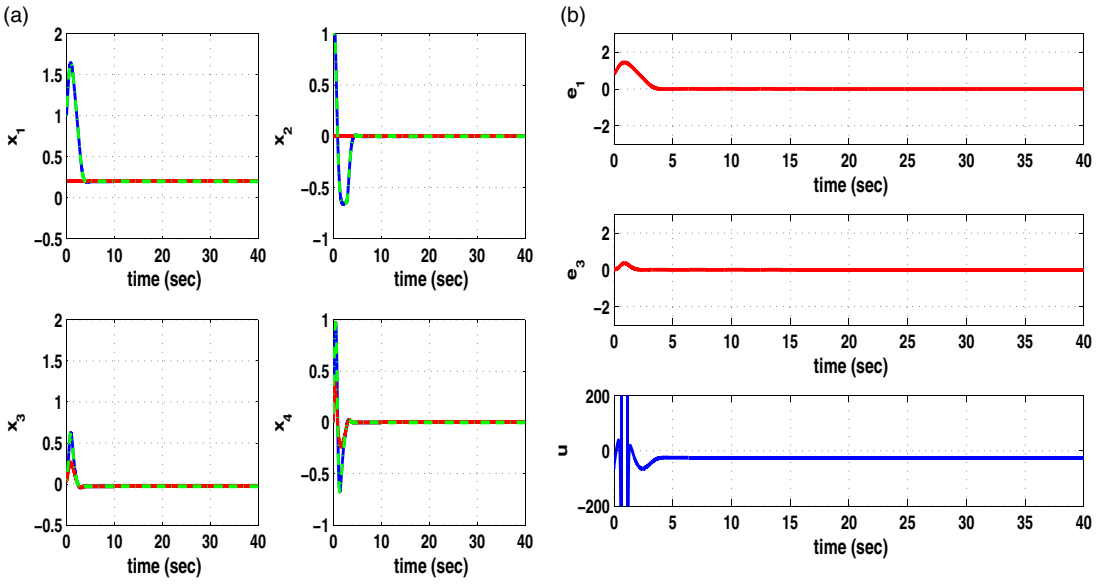


Figure 17. *Sliding-mode control of the PLI robot when tracking setpoint 2: (a) state variables x_i $i = 1, \cdots, 4$ (blue lines), their estimated values (green lines) and the associated reference setpoints (red lines), (b) tracking errors e_1 (state variable x_1) and e_2 (state variable x_3) and control input u of the PLI robot.*

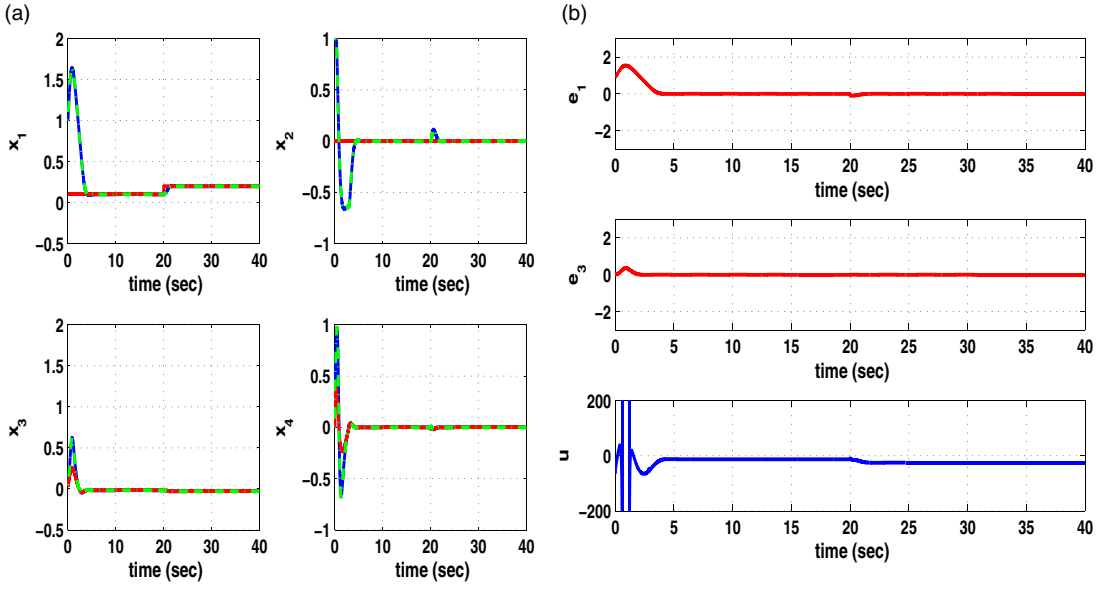


Figure 18. *Sliding-mode control of the PLI robot when tracking setpoint 3: (a) state variables x_i $i = 1, \cdots, 4$ (blue lines), their estimated values (green lines) and the associated reference setpoints (red lines), (b) tracking errors e_1 (state variable x_1) and e_2 (state variable x_3) and control input u of the PLI robot.*

https://doi.org/10.1017/S026357472100148X Published online by Cambridge University Press

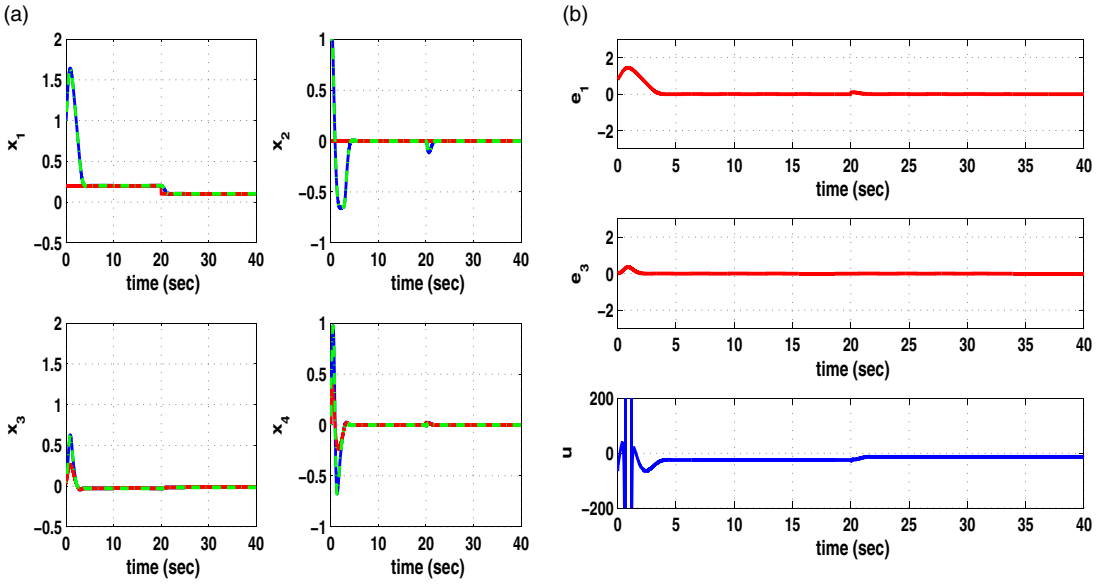


Figure 19. *Sliding-mode control of the PLI robot when tracking setpoint 4: (a) state variables x_i $i = 1, \cdots, 4$ (blue lines), their estimated values (green lines) and the associated reference setpoints (red lines) (b) tracking errors e_1 (state variable x_1) and e_2 (state variable x_3) and control input u of the PLI robot.*

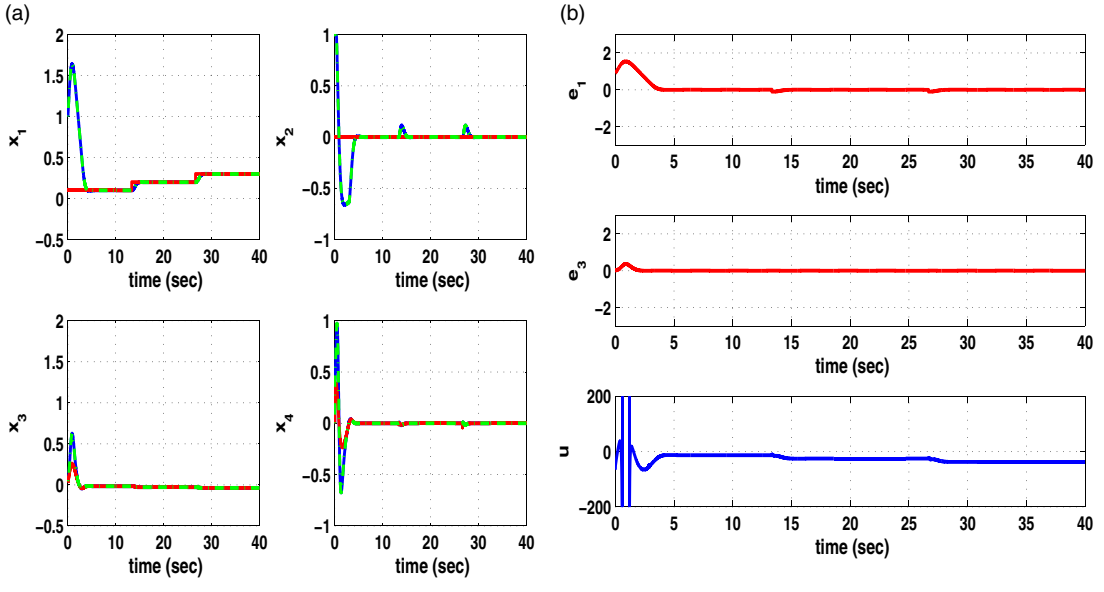


Figure 20. *Sliding-mode control of the PLI robot when tracking setpoint 5: (a) state variables x_i $i = 1, \cdots, 4$ (blue lines), their estimated values (green lines) and the associated reference setpoints (red lines) (b) tracking errors e_1 (state variable x_1) and e_2 (state variable x_3) and control input u of the power-line inspection robot.*

https://doi.org/10.1017/S026357472100148X Published online by Cambridge University Press

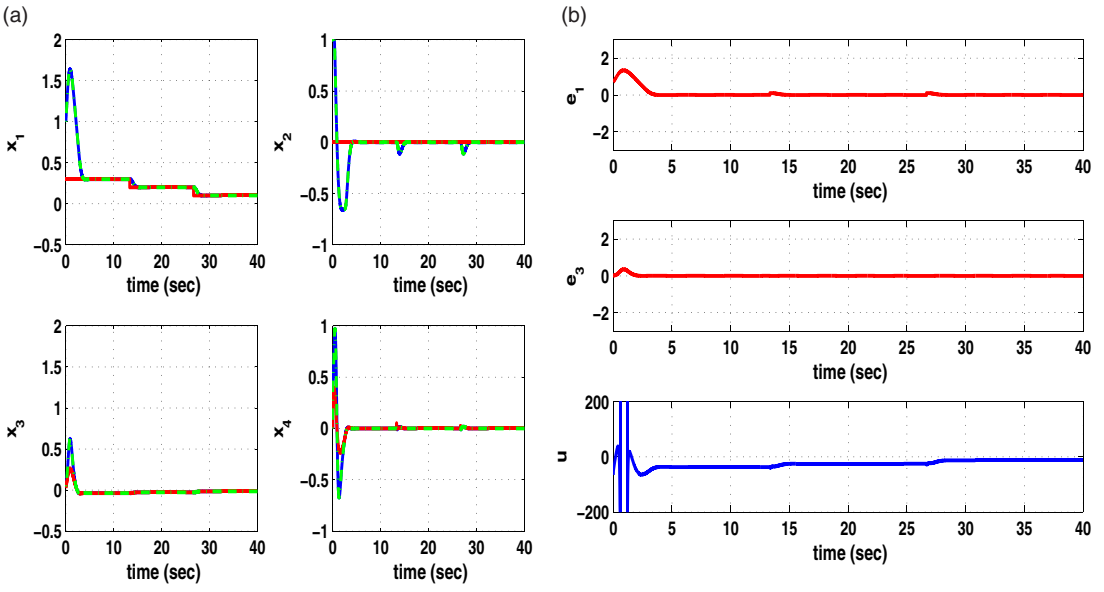


Figure 21. *Sliding-mode control of the power-line inspection robot when tracking setpoint 6: (a) state variables x_i $i = 1, \cdots, 4$ (blue lines), their estimated values (green lines) and the associated reference setpoints (red lines), (b) tracking errors e_1 (state variable x_1) and e_2 (state variable x_3) and control input u of the power-line inspection robot.*

Remark 2: Although NMPC is a popular approach for implementing optimal control in industrial and robotic systems, the method's performance is not always proven, while the performance of its iterative search for an optimum is dependent on ad-hoc selection of the values of specific parameters. On the other side, the application of the back-stepping control method as presented in [1] requires some transformations and simplifications of the state-space model of the power-line inspection robot, so as to obtain finally a description in the back-stepping integral (strict-feedback) form. Additionally, the application of flatness-based control requires to prove first the differential flatness properties of the dynamic model of the power-lines inspection robot. This is enabled only after some changes and simplifications are performed in the initial nonlinear model of the robot, as described in Section 5. Equivalently, to apply sliding-mode control to the dynamic model of PLI robots, the selection of sliding surfaces is in general an intuitive procedure. Only after transformation in the state-space form of Section 5.1 there exists a well-defined procedure for defining sliding surfaces and for implementing sliding-mode control.

8. Conclusions

A nonlinear optimal (H-infinity) control method has been developed for the dynamic model of a power-lines inspection robot. Control and stabilization of this type of robot is a nontrivial problem because of the nonlinear dynamics of the robotic mechanism, as well as because of underactuation. Actually, the considered robotic system has two degrees of freedom while receiving only one control input. To achieve a solution for this control problem, the dynamic model of the PLI robot has undergone first approximate linearization around a time-varying operating point which was updated at each time-step of the control method. The linearization process relied on first-order Taylor series expansion and on the computation of the related Jacobian matrices.

For the approximately linearized model of the PLI robot an H-infinity feedback controller was designed. To compute the controller's gains an algebraic Riccati equation was repetitively solved at each iteration of the control algorithm. The global stability properties of the control scheme were proven

https://doi.org/10.1017/S026357472100148X Published online by Cambridge University Press

through Lyapunov analysis. The proposed nonlinear optimal (H-infinity) control method retains the advantages of linear optimal control, that is fast and accurate tracking of reference setpoints under moderate variations of the control inputs. The method has been also compared against flatness-based control and sliding-mode control. The benefit from the application of the nonlinear optimal control method is in assuring the precise functioning of the PLI robot under minimal dissipation of energy by its actuators. Such a type of robots can release the power grid's maintenance personnel from dangerous tasks related with the inspection of overhead cables of the power transmission and distribution system.

References

[1] S. Dian, L. Chen, S. Hoang, M. Pu and J. Liu, "Dynamic balance control based on an adaptive gain-scheduled backstepping scheme for power-line inspection robots," *IEEE/CAA J. Automat. Sin.* **6**(1), 198–208 (2019).

[2] Z. Li and R. Yuan, "Autonomous inspection robot for power transmission lines maintenance while operating on the overhead ground wires," *J. Adv. Robot. Syst.* **7**(4), 107–113 (2010).

[3] L. Chen, G. Liu, H. Dong, S. Hoang and S. Dion, "Position Control on Center of Mass for Power Line Inspection Robot," *IEEE CCC 2016, Proc. of the 35th Chinese Control Conference,* Chengdu, China (2016)

[4] Z. He, W. Wang, H. Ruan, Y. Yao and X. Li, "A two-wheel load balance control strategy for an HVTL inspection robot based on second-order sliding-mode," *Ind. Robot* **46**(1), 83–92 (2019).

[5] A. B. Alhassan, X. Zhang, H. Shen and H. Xu, "Power transmission line inspection robots: A review, trends and challenges," *Electr. Power Energy Syst.* **118**, 105862–105880 (2020).

[6] H. Seki, S. Nakayama, K. Uenishi, T. Tsuji, M. Hikizu, Y. Makino, A. Kakiuchi and Y. Kanda, "Development of assistive robotic arm for power line maintenance," *Precis. Eng.* **67**, 69–76 (2021).

[7] L. Wang and H. Wang, "A Survey on Insulator Inspection Robot for Power Transmission Lines," *IEEE CARPI 2016, IEE 2016 4th Inlt. Conference on Applied Robotics for the Power Industry*, Jinan, China (2016).

[8] J. Y. Park, J. K. Lee, B. H. Cho and K. Y. Oh, "An inspection robot for live-line suspension insulator strings in 345 kV power lines," *IEEE Trans. Power Delivery* **27**(2), 632–639 (2012).

[9] N. Pouliot, P. L. Richard and S. Montabault, "LineScout Technology opens the way to robotic inspection and maintenance of high-voltage power lines," *IEEE Power Energy Technol. Syst. J.* **2**(1), 1–10 (2015).

[10] N. Pouliot and S. Montamabault, "Geometric Design of the LineScout, A Teleoperated Robot for Power Line Inspection and Maintenance," *200 IEEE Intl. Conference on Robotics and Automation*, Pasadena, California, USA (2009).

[11] P. Debenest, M. Guarnieri, K. Takita, E. F. Fukushima, S. Hirose, K. Tamura. A. Kimura, H. Kubokawa, N. Iwama and F. Shiga, "Expliner – Robot for Inspection of Transmission Lines," *IEEE ICRA 2008, IEEE 2019 Intl. Conference on Robotics and Automation,* Pasadena, California, USA (2008).

[12] T. Zhao, J. Liu, S. Dian, R. Guo and S. Li, "Sliding-mode-control-theory-based adaptive general type-2 fuzzy neural network control for power-line inspection robots," *Neurocomputing* **401**, 281–229 (2020).

[13] D. Yang, Z. Feng, X. Ren and N. Lu, "A novel power line inspection robot with dual-parallelogram architecture and its vibration suppression control," *J. Adv. Robot.* **28**(12), 807–819 (2014).

[14] G. Notomista, Y. Emam and N.M. Egerstedm, "The Slothbot: A novel design for a wire-traversing robot," *IEEE Robot. Automat. Lett.* **4**(2), 1993–1998 (2019).

[15] D. Yang, Z. Feng, R. Sha and X. Ren, "Robust control of a class of under-actuated mechanical systems with model uncertainty," *Intl. J. Cont.* **92**(7), 1567–1579 (2018).

[16] K. H. Seok and Y. S. Kim, "A state-of-the-art of power transmission for maintenance robots," *J. Electric. Eng. Technol.* **11**(5), 1412–1422 (2016).

[17] W. Chang, G. Yang, J. Yu, Z. Liang, L. Cheng and C. Zhou, "Development of a Power Line Inspection Robot with Hybrid Operation Modes," *IEEE/RSJ 2017, IEEE 2017 Intl. Conference on Intelligent Robots and Systems*, Vancouver, Canada (2017).

[18] H. Wang, B. Yan, Z. Pu, Y. Xiang, Q. Fan, J. Li and L. Zheng, "Optimal design and stress analysis of the transmission line inpsection robot along the ground line," *IET J. Eng. (Proc. of the 1th Intl Conf. on AC and DC Power Transmission, IET ACDC 2018)* **16**, 2088–3091 (2019).

[19] W. Jiang, Y. Yan, L. Yu, M. Peng, H. Li and W. Chen, "Research on dual-arm coordination motion control strategy for power cable mobile robot," *Trans. Inst. Meas. Cont.* **41**(11), 3235–3247 (2019).

[20] E. Boje, "Attitude and Position Estimation for a Power Line Inspection Robot," *Proc. 7th IFAC Symposium on Mechatronic Systems, IFAC Mechatronics 2016,* Loughborough, UK (2016).

[21] Y. Gao, G. Song, S. Li, F. Zhen, D. Chen, and A, Song, "LineSpyX: A Power Line Inspection Robot Based on Digital Radiography," *2020 IEEE/RSJ International Conference on Intelligent Robots and Systems (IROS)* (Oct. 2020), Las Vegas, NV, USA.

[22] H. Shen, X. Zhang, A. B. Alhassan, J. Gup and H. Xu, "Research on the Coupling Model for Inspection Robot to Depart from High-Voltage Transmission Line," *IEEE 2018 Intl. Conference on Sensing, Diagnostics, Prognostics and Control, IEEE SDPC 2018*, Xian, China (2018).

[23] N. Morozovsky and F. Bewley, "SkySweeper: A low DOF dynamic high wire robot," *IEEE Robot. Automat. Lett.* **4**(2), 1993–1998 (2019).

https://doi.org/10.1017/S026357472100148X Published online by Cambridge University Press

[24] H. Wang, F. Zhang, Y. Jiang, G. Liu and X. Peng, "Development of an Inspection Robot for 500kV EHV Power Transmission Lines," *IEEE/RSJ 2010, IEEE 2010 Intl. Conference on Intelligent Robots and Systems*, Taipei, Taiwan (2010).
[25] G. Rigatos and K. Busawon, *Robotic Manipulators and Vehicle: Control, Estimation and Filtering*, Springer (2018).
[26] X. Yue, H. Wang and J. Jiamg, "A novel 110 kV power line inspection robot and its climbing stability analysis," *Intl. J. Adv. Robot. Syst.* **14**(3), 1–10 (2017).
[27] S. Dian, C. Lin, S. Hoang, T. Zhao and J. Tan, "Gain-scheduled dynamic surface control for a class of underactuated mechanical systems using neural network disturbance onserver," *Neurocomputing* **275**, 1998–2008 (2018).
[28] L. Guo, X. Mo and Y. Song, "Dynamic Modelling and Adaptive Controller Design for a Wire-Moving Robot," *IEEE CCC 2015, Proc. of the 34th Chinese Control Conference,* Hangzhou, China (2015).
[29] O. Menendez, F. Auat Cheein, M. Perez and S. Koura, "Robotics in power systems," *IEEE Ind. Electron. Mag.* **11**(2), 22–34 (2017)
[30] F. Zhang, G. Liu, L. Fang and H. Wang, "Estimation of battery state of charge woth observer: Applied to a robot for inspecting power transmission lines," *IEEE Trans. Ind. Electron.* **59**(2), 1086–1097 (2012).
[31] G. G. Rigatos and S. G. Tzafestas, "Extended Kalman filtering for fuzzy modelling and multi-sensor fusion," *Math. Comput. Model. Dyn. Syst.* **13**, 251–266 (2007).
[32] M. Basseville and I. Nikiforov, *Detection of Abrupt Changes: Theory and Applications* (Prentice-Hall, 1993).
[33] G. Rigatos and Q. Zhang, "Fuzzy model validation using the local statistical approach," *Fuzzy Sets Syst.* **60**(7), 882–904 (2009).
[34] G. Rigatos, *Intelligent Renewable Energy Systems: Modelling and Control* (Springer, 2016).
[35] G. Rigatos, P. Siano and C. Cecati, "A new non-linear H-infinity feedback control approach for three-phase voltage source converters," *Electr. Power Comp. Syst.* **44**(3), 302–312 (2015).
[36] G. Rigatos, P. Siano, P. Wira and F. Profumo, "Nonlinear H-infinity feedback control for asynchronous motors of electric trains," *J. Intell. Ind. Syst.* (2015)
[37] G. Rigatos, *Nonlinear Control and Filtering Using Differential Flatness Theory Approaches: Applications to Electromechanical Systems* (Springer, 2015).
[38] G. J. Toussaint, T. Basar and F. Bullo, Optimal Tracking Control Techniques for Nonlinear Underactuated Systems," *Proc. IEEE CDC 2000, 39th IEEE Conference on Decision and Control,* Sydney Australia (2000).
[39] G. Rigatos, K. Busawon, J. Pomares and M. Abbaszadeh, "Nonlinear optimal control for the wheeled inverted pendulum system," *Robotica* **38**(1), 29–47 (2020).
[40] R. W. Beard and T. W. Mclain, "Successive galerkin approximation algorithms for nonlinear optimal and robust control," *Int. J. Cont.* **71**(5), 717–743 (1998).
[41] M. Rahaghi, and F. Barat, "Solving nonlinear optimal path tracking problem using a new closed loop direct–indirect optimization method: Application on mechanical manipulators," *Robotica* **37**(1), 39–61 (2019).
[42] A. Siqueira and M. Terra, "Nonlinear H-infinity controllers for underactuated cooperative manipulators," *Robotica* **25**(4), 425–432 (2020).
[43] L. G. Lin and M. Xin, "Computational Enhancement of the SDRE Scheme: General Theory and Robotic Control System," *IEEE Trans. Robot.* **36**(3), 875–993 (2020).
[44] Z. Zhonglin, F. Bin, L. Liquan and Y. Encheng, "Design and function realization of nuclear power inspection robot system," *Robotica* **39**(1), 165–180 (2021).
[45] J. Katrasnik, F. Pernus and B. Likar, "A survey of mobile robots for distribution power line inspection," *IEEE Trans. Delivery* **25**(1), 485–493 (2010).
[46] W. Jiang, G. Ye, D. Zou and Y. Yan, "Mechanism configuration and innovation control system design for power cable line mobile maintenance robot," *Robotica* **39**(7), 1251–1263 (2021).
[47] W. Jiang, D. Zou, X. Zhou, G. Zuo, G. Cheng Ye and H. J. Li, "Research on key technologies of multi-task orientatedd live maintenance robots for Ultra High Voltage multi-slit transmission lines," *Ind. Robot* **48**(1), 17–28 (2001).
[48] Y. Yao, W. Wang, Y. Qiao, Z. He, F. Liu, X. Li and X. Liu, "A novel series-parallel hybrid robot for climbing transmission tower," *Ind. Robot* (2021).
[49] G. H. Farias dos Santos, M. H. Abdali, D. Martins and C. B. A. Alexandre, "Geometrical motion pplanning for cable-climbing robots applied to distribution power lines inspection," *Int. J. Syst. Sci.* **52**(8), 1646–1663 (2021).
[50] G. Silano, T. Baca, R. Penicka, D. Liuzza and M. Saska, "Power-line inspection tasks with multi-aerial robot systems via signal temporal logic specifications," *IEEE Robot. Automat. Lett.* **6**(2), 4169–4177 (2021).
[51] A. Suarez, R. Salmoral, P. J. Zarco-Perinan and A. Ollero, "Experimental evaluation of aerial manipulation robot in contact with 15KV Power Line: Shielded and long reach configurations," *IEEE Access* **9**, 94573–94585 (2021).
[52] H. Guan, X. Sun, Y. Su, T. Hu, H. Wang, C. Peng and Q. Guo, "UAV-lidar aids automatic intelligent powerline inspection," *Intl. J. Electr. Power Energy Syst.* **130**, 106987–106997 (2021).
[53] R. S. Goncalves and J. C. M. Carvalho, "Review and latest trends in mobile robots used on power transmission lines," *J. Adv. Robot. Syst.* **10**, 1–14 (2013).
[54] G. Rigatos, "Differential flatness theory-based control and filtering for a mobile manipulator," *J. Cybern. Phys.* **9**(1), 57–68 (2020).

Cite this article: G. Rigatos, N. Zervos, P. Siano, M. Abbaszadeh, J. Pomares and P. Wira (2022). "A nonlinear optimal control approach for underactuated power-line inspection robots", Robotica **40**, 1979–2009. https://doi.org/10.1017/S026357472100148X

https://doi.org/10.1017/S026357472100148X Published online by Cambridge University Press